


Cite this: *Nanoscale*, 2024, 16, 3393

## Methanol recovery: potential of nanolaminate organic solvent nanofiltration (OSN) membranes†

Tuğba Baysal, <sup>a</sup> Aysa Güvensoy-Morkoyun, <sup>b</sup> Ş. Birgül Tantekin-Ersolmaz <sup>\*b,c</sup> and Sadiye Velioglu <sup>\*a,d</sup>

Researchers have made a significant breakthrough by merging the energy-saving attribute of organic solvent nanofiltration (OSN) with the remarkable solvent permeance and solute rejection of two-dimensional (2D) laminated membranes. This innovative approach brings forth a new era of sustainable and cost-effective separation techniques, presenting a promising solution to the issue of industrial solvents contaminating the environment. This development paves the way for new opportunities in building a sustainable future. Specifically, our mini-review has cast a spotlight on the separation and recovery of methanol—a solvent abundantly used in industrial processes. We systematically evaluated a diverse array of free-standing 2D nanolaminate OSN membranes. The analysis encompasses the assessment of pure methanol permeance, solute rejection capabilities, and the simultaneous evaluation of methanol permeance and solute rejection performance. Notably, this study sheds light on the considerable potential of 2D laminated OSN membranes in revolutionizing separation processes for the industrial use of methanol.

Received 5th November 2023,

Accepted 6th January 2024

DOI: 10.1039/d3nr05611b

rsc.li/nanoscale

### 1. Introduction

Organic solvents are a fundamental ingredient of organic synthesis in various industries. The separation of the final products from these solvents is crucial. In industries such as chemicals, paints, fuels, textiles, food, and pharmaceuticals (Fig. 1a), solvent separation processes comprise a significant portion (40–70%) of the industry's capital and operational costs.<sup>1</sup> Unfortunately, conventional separation methods, such as distillation, evaporation, extraction, adsorption, crystallization, and chromatography, are all energy-intensive and economically challenging due to their high capital and operational costs.<sup>2</sup>

The Environmental Protection Agency (EPA) has reported that in 2019, approximately 73 million tons of solvents were utilized in waste management operations, including recycling, treatment, combustion, and disposal in the United States (Fig. 1b). Notably, nearly 3 million tons of these solvents were released into the environment without undergoing purification, implying the inefficiency of conventional separation techniques.<sup>3</sup> On a global scale, this situation poses an increasingly significant threat as waste levels continue to increase steadily. Furthermore, the release of organic solvents into the environment endangers the health of all living organisms.<sup>4</sup>

Methanol is one of the most widely used solvents in industrial applications, followed closely by cumene, toluene, dichloromethane, and *n*-hexane. Unfortunately, a significant amount of methanol is released into the environment as waste. For example, in the United States alone, around 14 million tons of methanol were used for waste management in 2019 (Fig. 1b), with 818 258 tons being released without proper purification (EPA, 2019). It is inevitable that the total will exceed this value, considering the number of countries around the world. Therefore, it is crucial to reuse, recover, and recycle large amounts of methanol for both economic and environmental sustainability. Interestingly, in many industries today, the costs associated with recycling and disposing of solvents are nearly equivalent to the costs of purchasing new solvents.<sup>1</sup> Considering the detrimental effects of organic solvents on the economy, environment, and human health, the development of an efficient method is required to separate and recover these substantial waste volumes.

<sup>a</sup>Institute of Nanotechnology, Gebze Technical University, Gebze, Kocaeli, 41400, Türkiye. E-mail: sadiyevelioglu@gtu.edu.tr

<sup>b</sup>Department of Chemical Engineering, Istanbul Technical University, Maslak, Istanbul, 34469, Türkiye. E-mail: ersolmaz@itu.edu.tr

<sup>c</sup>Synthetic Fuels & Chemicals Technology Center (SENTEK), Istanbul Technical University, Maslak, Istanbul, 34469, Türkiye

<sup>d</sup>Nanotechnology Research and Application Center (NUAM), Gebze Technical University, Gebze, Kocaeli, 41400, Türkiye

† Electronic supplementary information (ESI) available: Table S1 presents comprehensive information on individual studies, encompassing details such as the authors' names, publication titles, and related information, as well as the methanol permeance with and without solute, and the solute rejection rates and Table S2 tabulates the ratio of pure methanol permeance (PMP) over pure water permeance (PWP) of free-standing 2D nanolaminate membranes (excel file). See DOI: <https://doi.org/10.1039/d3nr05611b>

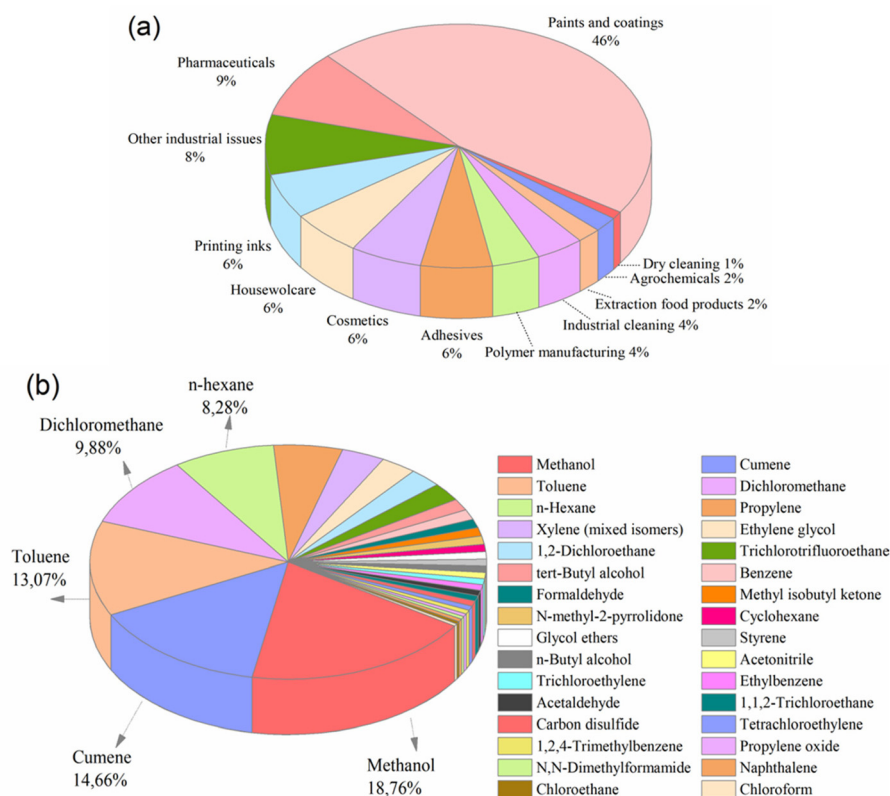


Fig. 1 (a) Solvent use arranged by sector,<sup>5</sup> and (b) solvents released and waste-managed in USA, 2019 (total amount: 72 594 759 tons per year).<sup>3</sup>

Organic solvent nanofiltration (OSN) is a revolutionary separation process that promises to replace traditional methods. Unlike thermal methods, OSN requires minimal energy and can separate even the most temperature-sensitive compounds at ambient conditions. This makes OSN an economically viable option for large-scale industrial applications, as it significantly reduces energy consumption while maintaining

high yields. Moreover, OSN is easy to install and operate, with low capital and operational costs. By effectively separating solutes based on either their size and molecular weight (a pore-flow mechanism) or their sorption and diffusion capacity (solution-diffusion mechanism), OSN proves to be a cost-effective and environmentally friendly solution with a lower carbon footprint than other separation processes.<sup>6</sup>



Tuğba Baysal

*Tuğba Baysal is a dedicated Research Assistant and a Ph.D. candidate in the Institute of Nanotechnology at Gebze Technical University. She received her B.Sc. degree in Chemical Engineering at Yıldız Technical University and her M. Sc. degree in Nanoscience and Nanoengineering at Istanbul Technical University. Her research is primarily centered around membrane technology,*

*with a specific focus on organic solvent nanofiltration. Furthermore, she conducts in-depth investigations involving atomistic-scale simulations to advance the understanding and development of membranes for various separation applications.*



Aysa Güvensoy-Morkoyun

*Aysa Güvensoy-Morkoyun is a Ph.D. candidate and research/teaching assistant in the Department of Chemical Engineering at Istanbul Technical University. She received her B.Sc. degree with Majors in Chemical Engineering as well as Molecular Biology and Genetics and her M.Sc. degree in Chemical Engineering from Istanbul Technical University. Her research interests are mem-*

*brane-based desalination, organic solvent filtration, and molecular simulation of related nanomaterials.*

OSN technology has continuously advanced with research efforts focusing on innovative materials that aim at achieving high separation performance with good solute rejection, high solvent permeance, and long-term stability. Contrary to the limitations of conventional polymeric materials, breakthroughs in nanotechnology have prompted the design of novel membrane materials with abundant, uniform, and narrow pores in addition to low tortuosity. So far, various nanomaterials have been utilized in OSN, including 0D (graphene quantum dot, metal-based chalcogenide, nano-aggregate, *etc.*),<sup>7–9</sup> 1D (carbon nanotube, *etc.*), 2D nanomaterials (graphene, graphene oxide (GO), metal–organic framework (MOF), covalent organic framework (COF), hexagonal boron nitride (hBN), MoS<sub>2</sub>, MXene, *etc.*),<sup>10–16</sup> and 3D nanomaterials (MOF, zeolite, metal oxide, *etc.*).<sup>17,18</sup> Fortunately, the development of 2D nanomaterials has stimulated the fabrication of ultra-thin membranes with uniform nanopores/nanochannels.<sup>19–21</sup> Additionally, they have shown great potential for the separation and recovery of different solvents due to tailorability with functional groups and building blocks. The integration of these nanomaterials into membrane technology as either free-standing or nanocomposite membranes promises to provide enhanced performance that surpasses the existing permeability–selectivity trade-off of current commercial membranes. With these advancements, researchers have paved the way for the next generation of membranes, providing new opportunities for more efficient and sustainable separation technologies.

Our analysis will focus on the identification of notable free-standing 2D nanolaminate membranes, rather than hybrid or mixed matrix membranes, and examine their advantages in methanol separation. After providing a detailed explanation of the fundamental need for methanol separation and a comprehensive discussion of the general significance, benefits, and challenges of OSN and 2D membranes; elucidation of the separation mechanism of OSN membranes will be evaluated bene-

fitting from both polymeric and nanomaterial-based membranes. This review will aid in contextualizing the significance of 2D membranes and will serve as a basis for further understanding of the importance of methanol separation. Since there are different studies focused on different aspects of the 2D nanolaminate membrane's properties when compiling the literature, we ended up with three separate sections: one for paired parameters (solute rejection-methanol permeance) and two for unpaired parameters. To provide a comprehensive overview, we have divided the unpaired parameters into two separate sections. Collectively, this review aims to provide an elaborate analysis of 2D membranes in methanol separation and put 2D nanomaterials into perspective for niche separation applications.

## 2. The significance of methanol separation

Methanol, a significantly utilized compound with substantial environmental emissions (Fig. 1b), is a protic and highly polar alcohol. It falls within the polarity group of 2, as indicated by its Reichardt index of 0.762. Predominantly derived from natural gas, its annual production volume in 2020 reached approximately 157 million tons.<sup>4</sup> Its production is expected to double in 2030, with an anticipated output of 311 million tons, owing to the establishment of 131 new methanol plants.<sup>22</sup> Methanol exhibits pronounced toxicity upon ingestion and can induce poisoning through skin exposure above the specified concentration or inhalation of its vapor. Furthermore, its metabolic breakdown yields compounds such as formaldehyde, formic acid, and formate, which have severe effects on human health.<sup>4,23</sup> Given the numerous factors impacting the solvent selection, including their effects on health, environmental considerations, physical and chemical properties, production costs, and safety aspects (*e.g.*, explosion



**Ş. Birgül Tantekin-Ersolmaz**

*Ş. Birgül Tantekin-Ersolmaz is a Professor of Chemical Engineering at Istanbul Technical University. She received her BS degree from Istanbul Technical University (ITU) and MS and PhD degrees from the University of Colorado, Boulder, in chemical engineering. She leads the Membrane Separations Research Group of the ITU-SENTEK, Synthetic Fuels & Chemicals Technology Center at ITU. Her research interest lies*

*in the cross-sections of molecular separations, porous materials, and polymer and hybrid membranes for energy, water, and environmental applications.*



**Sadiye Velioglu**

*Sadiye Velioglu is an Associate Professor at the Institute of Nanotechnology, Gebze Technical University. She has completed post-doctoral fellowships at Istanbul Technical University from 2015–2016, Nanyang Technological University in Singapore from 2016–2018, and Koç University in Türkiye from 2018–2019. She received the 2023 Outstanding Young Scientists Award (GEBİP) from the Turkish Academy of*

*Sciences (TÜBA). She specializes in membrane technology, with a specific focus on energy and environmental applications such as carbon capture, natural gas separation, water treatment, and organic solvent nanofiltration.*

risk and flammability), solvents are typically categorized into four principal groups: recommended, problematic, hazardous, and highly hazardous. Despite the adverse health effects associated with methanol, it is classified within the recommended solvent category, considering its all attributes.<sup>24</sup>

Methanol is a compound that can be produced industrially through catalytic reactions of CO and H<sub>2</sub>, or *via* fermentation of biomass. Its versatility makes it useful as a solvent, anti-freeze, fuel, and as a key raw material for the production of various chemicals and materials. It finds extensive applications in multiple industries such as construction, automotive, electronics, appliances, paints and coatings, insulation, pharmaceuticals, and packaging. However, due to its high utilization, it is often released in significant amounts into the environment, causing pollution. According to the EPA report, methanol is the highly utilized solvent in waste management practices, with substantial release into the environment (Fig. 2).<sup>4</sup> Fig. 2a and c present a detailed breakdown of the percentages of methanol employed for waste management across various industrial sectors and the cumulative methanol waste generated in the USA for the years 1995 and 2019, respectively.

Notably, over the course of nearly a quarter-century, the quantity of methanol allocated for waste management witnessed a remarkable two-order-of-magnitude increase, altering from 149 252 tons to approximately 13 million tons. Unfortunately, a large amount of waste methanol remains unutilized and is discharged. Specifically, Fig. 2b and d display the quantities of methanol released by various industries within the United States in 1995 and 2019, respectively. The expansion of industries that incorporate methanol in their processes, driven by technological advancements, has contributed to a substantial increase in the volume of released waste methanol over the years. The amount of methanol released to the environment increased from 93 965 tons (1995) to 818 258 tons (2019). Unfortunately, it is discharged into diverse environments, including air, water, underground, and land, with increasing discharged amounts to the air (Fig. 2e and f).<sup>4</sup> However, this rise in methanol release highlights the lack of efficient and cost-effective methanol separation processes.

It is worth noting that Fig. 2 exclusively illustrates the quantities of methanol utilized in waste management or discharged into the environment only in the United States for a particular

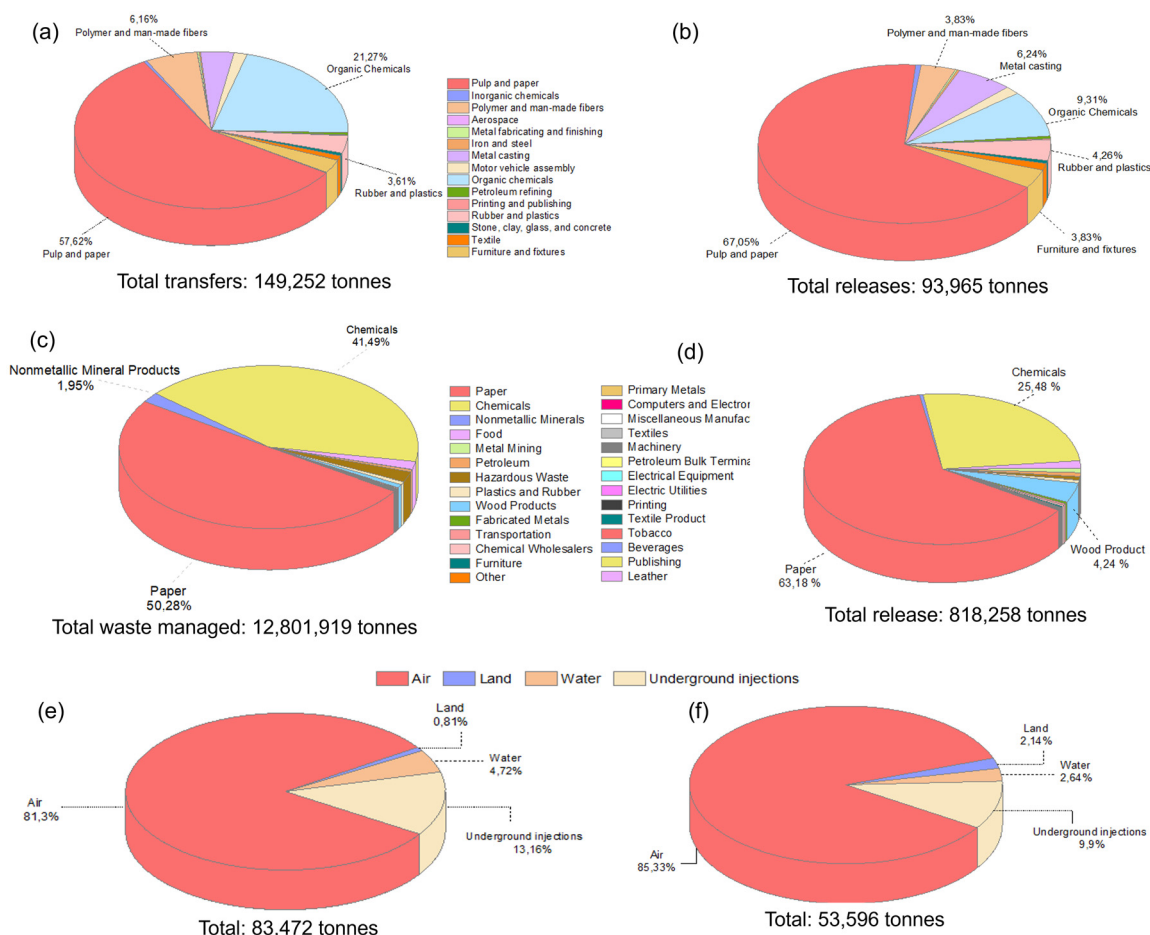


**Fig. 2** The percentage of methanol (a) transferred for treatment and disposal, and (b) released from various industries within the USA in 1995. The percentage of methanol (c) transferred for treatment and disposal, and (d) released from various industries within the USA in 2019. The percentage of methanol released to different environments in the USA in (e) 1993 and (f) 2016.<sup>4</sup>



year. On a global scale, the cumulative volume of methanol released, and waste managed assumes excessive proportions. The necessity for the efficient recovery, recycling, and reuse of such substantial methanol quantities becomes evident, not only from an economic standpoint but also due to its profound environmental significance.

### 3. Organic solvent nanofiltration (OSN) technology

Conventional solvent separation methods, including distillation, evaporation, extraction, adsorption, crystallization, and chromatography, have a vital role in various industries. However, they involve significant costs, amounting to 40–70% of an industry's capital and operational expenses.<sup>1</sup> However, organic solvent nanofiltration (OSN) is a highly promising separation process that has emerged as a viable alternative to these traditional separation methods. OSN utilizes a membrane to selectively separate and concentrate components in organic solvents, operating under a pressure of 5 to 40 bar.<sup>1</sup> With the ability to retain 0.1 to 2 nanometer-sized solutes, OSN has found widespread application in various industries, including pharmaceuticals, fine chemicals, petrochemicals, dyes, food and beverages, and cosmetics. Its usage is diverse, ranging from purifying and isolating pharmaceutical intermediates and active pharmaceutical ingredients (APIs) to removing dyes and recovering valuable solvents in the dye industry. OSN is also utilized in the concentration of flavors, fragrances, and natural extracts in the food industry.<sup>25</sup> The potential for isomer separation with OSN is also considered an area of future development in chemical engineering and polymer science.<sup>26</sup> With its versatility, OSN is quickly becoming a popular choice for industries seeking to optimize their separation processes.

The main reason for preferring OSN in many separation processes is its ability to allow for selective separation of

specific components and precise concentration of target molecules by tailoring the membrane surface. This capability enables efficient recovery and recycling of valuable solvents, leading to reduced waste generation and improved sustainability. OSN, whose performance evaluation is performed based on solvent permeance and solute rejection, offers a considerable separation efficiency. Additionally, OSN stands out with its remarkable energy efficiency, which is generally related to economic costs. Operating at lower temperatures, it requires less energy compared to traditional distillation processes as illustrated in Fig. 3 where OSN seems to require only pump energy to operate, while distillation requires high heating energy for phase transformation and separation. This obvious difference in energy requirements (3 MJ for OSN *versus* 1750 MJ for distillation) further highlights the energy efficiency of OSN.<sup>1</sup> Similarly, Kim *et al.*<sup>27</sup> compared the energy required to recover solvent by distillation and OSN. The study revealed a substantial difference in energy requirements, reaching as high as four orders of magnitude and being particularly evident in methanol recovery (150 kW h for distillation compared to 0.023 kW h for OSN). On the other hand, the cost of the process is also related to the loss of high-value-added products. Purification of active pharmaceutical ingredients (APIs), one of the highest value-added products in the pharmaceutical industry, is only one of the important applications that draws attention to the advantages of OSN. Székely *et al.*<sup>28</sup> compared OSN with recrystallization and flash chromatography, which are commonly used for the purification of APIs in the pharmaceutical industry. The removal of two toxic impurities from one API species in dichloromethane (DCM) was targeted using three different processes. Székely *et al.*<sup>28</sup> reported that OSN met the standards for the removal of both toxic impurities with ~6% API loss. Over 99.7% toxic impurity removal was achieved by chromatography. However, API loss increases to 12%, twice that of OSN. When recrystallization is used, the API loss is even higher for both toxic impurities (~16%). According

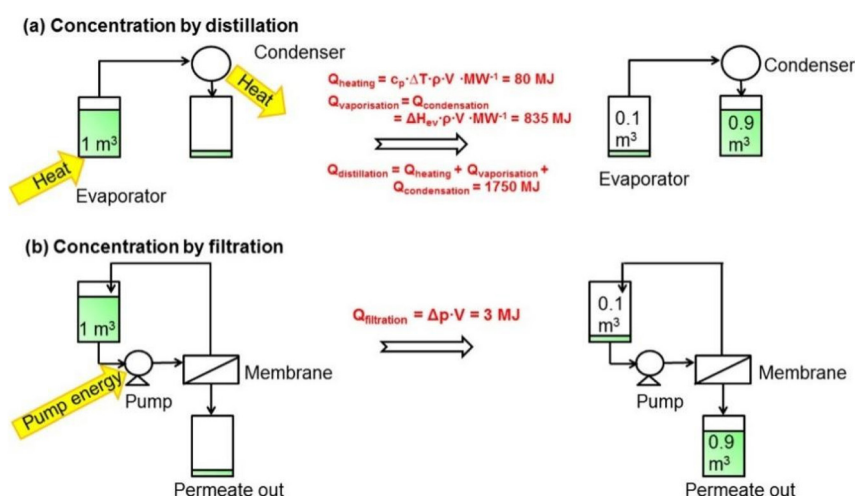


Fig. 3 Comparison of consumed energy by (a) distillation and (b) OSN processes to concentrate 1 m<sup>3</sup> of a dilute solution in methanol by a factor of 10.<sup>1</sup> This figure has been reproduced from ref. 1 with permission from American Chemical Society, Copyright 2014.

to this study, the main factor affecting the cost of processes was API loss. Furthermore, OSN is particularly advantageous for separating temperature-sensitive compounds, making it a valuable tool in various industries.<sup>1,25</sup>

This innovative procedure was eventually applied in manufacturing, addressing a significant revenue loss. Sereewatthanawut *et al.*<sup>29</sup> collaborated with Johnson & Johnson to investigate DuraMem membranes for extracting five distinct APIs from tetrahydrofuran (THF) and two different dyes, Solvent Yellow 7 (SY7,  $M_w$  198.2 g mol<sup>-1</sup>) and Brilliant Blue R (BBR,  $M_w$  826.0 g mol<sup>-1</sup>) from *N,N*-dimethylformamide (DMF). They achieved a final product having a purity of 99.7% with a 90% recovery of SY7. Moreover, 99% of the large oligomeric impurities (such as tetramer and higher) were successfully removed from the API-intermediate (API-INT) of a new drug candidate. This resulted in 99% API-INT recovery and reduction of oligomeric impurities in the synthesis solution from 6.8 to 2.4 wt%, which is below the allowed limit of 3 wt% for oligomeric impurities. OSN process led to a significant 200-fold decrease in energy usage when compared to distillation. Similarly, Rundquist *et al.*<sup>30</sup> investigated the OSN process on both lab- and pilot-scale for the recovery of API from mother liquors supplied by GlaxoSmithKlein Jurong R&D pilot plant. They reported an approximately 90% recovery rate in five different solvents for StarMem and PuraMem commercial membranes. Additionally, energy calculations revealed that OSN requires 25 times less energy per liter of solvent compared with distillation for solvent recovery.

For the successful operation of the OSN process, several factors need specific attention (Table 1). The first and most important factor is the OSN membrane material, which forms the heart of the OSN processes since the study of OSN membranes presents a complex and challenging effort. Membranes must have high solvent permeance and solute rejection as well

as good mechanical, thermal, and chemical stability. The second factor is the production of high-packing density modules to observe a larger membrane surface area per unit volume for the improvement in the productivity of the process. The final factor is the process design, which includes optimization of operating conditions, development of new membrane configurations, and integration of the membrane process with other unit operations. Since this review involves the evaluation of the effectiveness of 2D laminated membranes in the separation of methanol, we have only concentrated on the first factor in the OSN process. Specifically, solvent separation in the OSN process is predominantly governed by the intricate interplay of triple interactions among the solute, solvent, and membrane. These interactions are rooted in the collective influence of multiple parameters, as tabulated in Table 1. Consequently, any changes in the properties of the membrane, solute, or solvent components will inherently impact the overall performance of the separation process.<sup>31</sup>

## 4. 2D nanolaminate OSN membranes

The membrane industry employs a diverse range of materials for the fabrication of OSN membranes, encompassing both rigid and flexible polymers such as polyvinylidene fluoride, polysulfone, and polyacrylonitrile. In addition, 3D nanomaterials like zeolites, Al<sub>2</sub>O<sub>3</sub>, SiO<sub>2</sub>, TiO<sub>2</sub>, and ZrO<sub>2</sub>, as well as 2D nanomaterials like graphene, GO, COF, hexagonal boron nitride (hBN), MoS<sub>2</sub>, and MXene, have found applications in OSN membrane design.<sup>6,19,20,32</sup> Table 2 provides a brief overview of the advantages and drawbacks associated with each membrane material. Polymeric membranes are favored for their cost-effectiveness, ease of fabrication, and suitability for large-scale production. However, they exhibit certain stability

**Table 1** Parameters affecting OSN performance<sup>31</sup>

Process properties	Solvent properties	Solute properties	Membrane properties
Feed concentration	Molar volume	Solvated radii	Pore/channel size
Applied pressure	Polarity	Molecular weight	Pore/channel size distribution
Feed temperature	Viscosity	Molecular geometry	Porosity
Fluid dynamics	Surface tension	Solubility in solvent	Tortuosity
		Solubility in membrane	Hydrophilicity
		Charge	Surface energy

**Table 2** The pros and cons of each membrane material

Polymeric membranes	3D membranes	2D membranes
<ul style="list-style-type: none"> <li>• Low material price</li> <li>• Ease of fabrication</li> <li>• Stability problems (swelling, aging, and plasticization)</li> <li>• Low permeance</li> </ul>	<ul style="list-style-type: none"> <li>• High thermal, chemical, and mechanical stability</li> <li>• High perm-selectivity due to uniform pores</li> <li>• High material cost</li> <li>• Difficulty in upscaling</li> <li>• High mass transfer resistance</li> </ul>	<ul style="list-style-type: none"> <li>• Ultrathin membranes allow rapid solvent transportation due to low mass transfer resistance</li> <li>• Precise control over interlayer spacing or channels improves size-sieving ability</li> <li>• High material cost</li> <li>• Difficulty in upscaling</li> </ul>

**Table 3** Various intercalants and their effect on the *d*-spacing and separation performance

Intercalant name	2D material	<i>d</i> -Spacing enhancement <sup>a</sup> (Å)	Performance enhancement	Ref.
Iminodi(methyl phosphonic acid)	Ti <sub>3</sub> C <sub>2</sub> T <sub>x</sub>	12.2–13.1	2-Fold increase in water flux	36
Nitrilotri(methyl phosphonic acid)	Ti <sub>3</sub> C <sub>2</sub> T <sub>x</sub>	12.2–13.5	2.5-Fold increase in water flux	36
Phytic Asit	Ti <sub>3</sub> C <sub>2</sub> T <sub>x</sub>	12.2–16.5	5-Fold increase in water flux	36
Fe(OH) <sub>3</sub>	Ti <sub>3</sub> C <sub>2</sub> T <sub>x</sub>	13.71–14.47	10.6% increase in dye rejection	37
SO <sub>3</sub> H	Ti <sub>3</sub> C <sub>2</sub> T <sub>x</sub>	9.30–14.30	426.5% increase in dye adsorption	40
K <sup>+</sup>	MoS <sub>2</sub>	3.00–6.25 <sup>b</sup>	125% increase in water flux	41
Na <sup>+</sup>	MoS <sub>2</sub>	3.00–6.63 <sup>b</sup>	122% increase in water flux	41
Li <sup>+</sup>	MoS <sub>2</sub>	3.00–7.25 <sup>b</sup>	169% increase in water flux	41
Mg <sup>2+</sup>	MoS <sub>2</sub>	3.00–8.48 <sup>b</sup>	229% increase in water flux	41
Al <sup>3+</sup>	Ti <sub>3</sub> C <sub>2</sub> T <sub>x</sub>	13.50–14.70	17.1%–86.2% increase for K <sup>+</sup> , Na <sup>+</sup> , Ca <sup>2+</sup> , Mg <sup>2+</sup> ion rejections	35
Nano-Al <sub>2</sub> O <sub>3</sub>	Ti <sub>3</sub> C <sub>2</sub> T <sub>x</sub>	13.70–14.90	408% increase in water flux	42
STB	GO	7.67–13.47	56.6% increase in water flux	43

<sup>a</sup>To define *d*-space enhancement, *d*-spacing values before and after intercalation are given. <sup>b</sup> Interlayer distance.

issues over time. These issues include aging under high pressure, swelling in organic media, and plasticization due to the dissolution of penetrants. These complications can significantly impact the separation performance in terms of solvent permeance and solute rejection.<sup>6,33</sup> Therefore, nanomaterial-based membranes have emerged due to their robust mechanical, thermal, and chemical stability, as well as high separation efficiency. However, their manufacture has been limited by their high material cost, difficult processability, and inherent fragility. Within the nanomaterial family, 2D nanomaterial-based membranes are promising due to reducing mass transfer resistance and consequently enhancing permeance. They hold significant promise, offering a balance of elevated solute rejection due to their uniform nanopores/nanochannels.<sup>19,20</sup> Additionally, their performance is significantly impacted by their nanoscale size, rich chemistry, hydrophilicity, and electric charge.<sup>34</sup>

Recently, researchers have dominantly concentrated on tailoring the interlayer distance between 2D nanoplates. Specifically, they focused on exploring the use of various intercalants, such as K<sup>+</sup>, Al<sup>3+</sup>, and toluidine blue O (TBO), to enhance the performance of 2D OSN membranes.<sup>35</sup> These intercalants vary in size, shape, charge, and functionality, which alter the membrane properties. For instance, Yi *et al.*<sup>36</sup> employed organic phosphonic acids (OPAs) and phytic acid (PA), each containing various phosphonic acid groups, to expand the interlayer spacing of MXene. These active phosphonic acid groups effectively bonded with MXene layers through nucleophilic addition and condensation reactions, forming covalent Ti–O–P bonds at the interface. Membranes derived from this nanomaterial featured highly regular nanochannels and exceptional stability. In comparison to pure MXene membranes, the PA-modified MXene membrane exhibited a five-fold increase in solvent permeance without compromising dye rejection performance. Moreover, the PA-modified MXene membrane demonstrated remarkable stability, remaining structurally intact after immersion in both alkaline and acidic environments for approximately 24 days.

Not only solvent permeance improvement is achieved, but also solute rejection performance can be altered *via* intercala-

tion in 2D laminated membranes. For instance, Ding *et al.*<sup>37</sup> investigated the removal of dyes by adjusting the nanochannel width of 2D MXene OSN membranes with the introduction of Fe(OH)<sub>3</sub> nanoparticles. The modified membrane exhibited a remarkable water permeance of 1084 LMH bar<sup>−1</sup> and achieved an approximate 90% rejection performance for dyes with a molecular weight (*M<sub>w</sub>*) of 961 g mol<sup>−1</sup>. When tested with dyes of higher molecular weight (*M<sub>w</sub>*: 1364 g mol<sup>−1</sup>), the membrane maintained its high separation potential, with water permeance measured at 921 LMH bar<sup>−1</sup> and a 93% dye rejection. Similarly, Wang *et al.*<sup>38</sup> utilized TBO as an intercalant to modify the interlayer distance of GO. Surprisingly, despite the increased interlayer spacing, they achieved an impressive rejection performance of 99.9%, even for solutes with small molecular weights. This exceptional rejection was attributed to the presence of intercalants within the interlayer spacing, creating a diffusion barrier that effectively blocked solute passage. Although intercalants have primarily been used to improve solvent permeance, their ability to inhibit solute transport is also extremely encouraging and motivating. Table 3 provides an overview of different intercalant types, their effects on interlayer spacing, and their impact on separation performance. Additionally, it is noteworthy that intercalants have contributed significantly to the colloidal stability of 2D membranes, persisting between nanolayers even after extensive washing.<sup>39</sup>

## 5. Elucidating the separation mechanism of OSN membranes

### 5.1. Triple interactions between membrane–solvent–solute

Defining the precise transport mechanisms within OSN membranes remains a subject of ongoing research. The behavior of OSN membranes appears to exhibit dual characteristics, with some observations aligning with the solution–diffusion model, while others conform to the pore–flow model. Additionally, a thorough understanding of solute–solvent–membrane interaction is required to propose a reliable separation mechanism. However, the complexity of the triple interactions involving the

membrane, solute, and solvent poses a considerable challenge in accurately pinpointing these mechanisms. Addressing these complexities is vital for advancing our knowledge in the realm of OSN membranes.

In recent years, the assessment of solubility parameters ( $\delta_T$ ) has emerged as a valuable tool for evaluating the interactions between solvents, solutes, and membranes in solvent separation processes. In line with experimental research, theoretical studies, namely group contribution, molecular simulation, and machine learning approaches, have proven to be valuable and time-efficient methods for the calculation of solubility parameters. A noteworthy example of these approaches can be found in the work of Bastin *et al.*,<sup>44</sup> who employed a group contribution method to calculate the Hansen solubility parameters of polymeric membranes. The solubility parameters for solvents were taken from existing literature, while the solubility parameters for solutes (dyes) were determined using Fedors group contribution method,<sup>45</sup> particularly suitable for smaller molecules. The resulting solubility parameter values are detailed in Table 4. Of particular significance is the proximity of total solubility parameter values ( $\delta$ ), which offers insights into the strength of intermolecular interactions. Notably, in the case of acetonitrile (ACN) as the solvent, a high affinity was observed with all polymeric membranes. Consequently, the membranes experienced swelling and failed to demonstrate satisfactory separation performance. On the other hand, a close value of  $|\delta_{\text{solute}} - \delta_{\text{ACN}}|$  was expected to yield lower solute rejection performance. Because the increase in solvent–solute interactions enhances the drag effect of the solvent on solutes through the membranes, ultimately resulting in lower rejection performance.<sup>46</sup> This demonstrates the interplay between solubility parameters and membrane performance in the context of separation.

Mostly, it is not possible to accurately estimate the solubility parameters in cases where specific membrane materials are not accounted for in the group contribution database.<sup>13</sup> Alternatively, molecular simulation approaches offer a direct and robust pathway for the quantification of interaction energies among the membrane, solvent, and solute components. Moreover, these simulation techniques provide valuable information on the influence of these interactions on the overall separation performance of novel or unrepresented membrane

materials like recently emerging 2D nanomaterials. A study conducted by Li *et al.*<sup>47</sup> provides an illustrative example in which they engineered membranes with varying pore sizes and two different pore structures utilizing a MoS<sub>2</sub> membrane (see Fig. 4a). When utilizing a membrane characterized by pores lined with S edge atoms and featuring a pore width of 0.6 nm (coded as S\_0.6), the methanol flux measured  $3.5 \times 10^5 \text{ kg m}^{-2} \text{ h}^{-1}$ . In contrast, the employment of a membrane characterized by pores lined with Mo edge atoms and having a 0.7 nm pore width (coded as Mo\_0.7) resulted in a decreased methanol flux to  $2.1 \times 10^5 \text{ kg m}^{-2} \text{ h}^{-1}$  (Fig. 4b). This decline in methanol flux was attributed to the strong attraction of methanol by S atoms on the membrane pore edges and repulsion with Mo atoms as a result of the combined effect of vdW and Coulomb interactions (see Fig. 4c). These findings emphasize the critical role of repulsive or attractive interactions between the pore edges and the solvent, particularly in cases involving smaller pore dimensions. With further increase in pore diameter, methanol flux exhibited a linear relationship, irrespective of the pore structure. This behavior can be attributed to the diminished energy barrier between the solvent and the pore edge atoms at larger pore diameters, a phenomenon substantiated by the analysis of the potential of mean force (PMF). As a result, the energy barrier that methanol encountered while passing the pores of the membrane was proposed, and its effect on methanol transport was evaluated *via* molecular simulation methods. On the other hand, it has been clarified by molecular simulation studies that when considering transport through nanochannels in a 2D nanomaterial-based membrane (e.g. MXene, GO), the flow of solvents is affected by the arrangement of the solvents in the membrane with a low *d*-spacing value.<sup>48,49</sup> If the solvents are arranged in an ordered orientation, such as a single or bimolecular layer, the interaction energies between the solvent and the membrane surface increase, resulting in a higher flux. However, if the *d*-spacing increases, the interaction between the solvent and the membrane weakens, causing a random arrangement of solvents to occur. In this case, the properties of the solvent, such as its viscosity, play a more dominant role in determining the flux.

More recently, machine learning studies have begun to be employed to understand the interplay between membrane,

**Table 4** Solubility parameters for the solutes, solvent (ACN), and polymeric membranes used in the study of Bastin *et al.*<sup>44</sup>

Solutes (dyes)	$\delta_{\text{total}}^a$	$ \delta_{\text{solute}} - \delta_{\text{ACN}} $	$ \delta_{\text{solute}} - \delta_{\text{TBPEEK}} $	$ \delta_{\text{solute}} - \delta_{\text{PA}} $	$ \delta_{\text{solute}} - \delta_{\text{PSf}} $
Disperse red	25.0	0.6	0.8	0.1	2.0
Methyl orange	28.1	3.7	4.0	3.0	5.2
Safranin O	26.4	2.0	2.2	1.3	3.4
Crystal violet	20.4	4.0	3.7	4.7	2.5
Acid fuchsin	31.7	7.3	7.6	6.6	8.8
Rose bengal	32.8	8.4	8.6	7.7	9.8
$ \delta_{\text{ACN}} - \delta_{\text{membrane}} $			0.3	0.7	1.5

<sup>a</sup>The unit of solubility parameters are given in the unit of  $\text{MPa}^{1/2}$ . In the last row of the table, the solubility difference between ACN and membrane,  $|\delta_{\text{ACN}} - \delta_{\text{membrane}}|$ , is given where the relevant membrane type is represented in the corresponding column, namely TBPEEK, PA, and PSf, respectively. TBPEEK: poly(ether ether ketone); PA: polyamide; PSf: polysulfone.



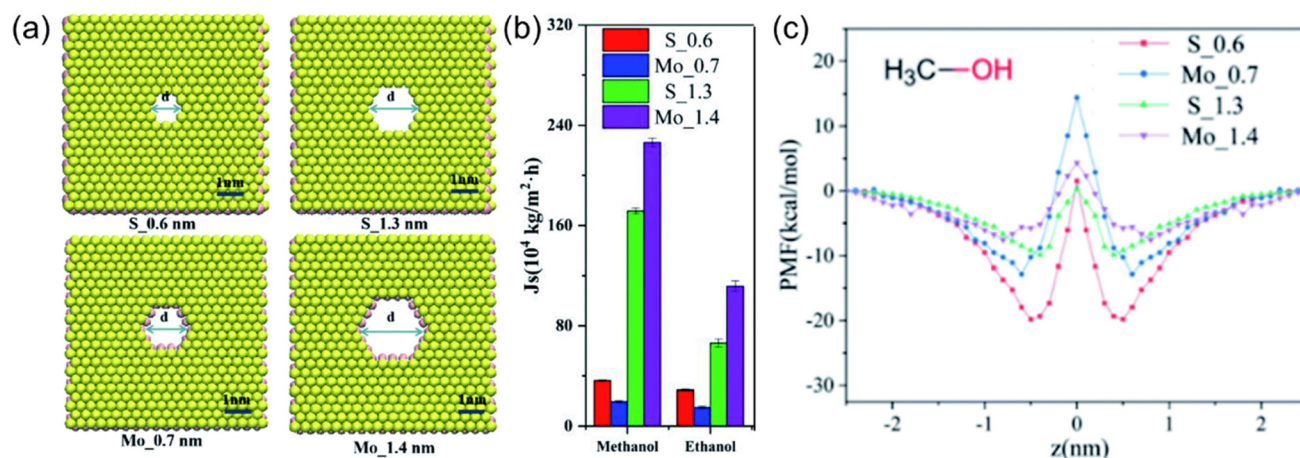


**Fig. 4** (a) Schematic representation of MoS<sub>2</sub> membranes with two different pore sizes and two different pore structures, (b) simulated flux of methanol through MoS<sub>2</sub> membranes, and (c) the PMFs of methanol in the MoS<sub>2</sub> pores (in b and c, red, blue, green, and purple lines and bars represent the data of S\_0.6, Mo\_0.7, S\_1.3, and Mo\_1.4 membranes, respectively).<sup>47</sup> This figure has been reproduced from ref. 47 with permission from The Royal Society of Chemistry, Copyright 2022.

solvent, and solute in OSN as an alternative to molecular simulation approaches. To illustrate, Ignacz *et al.*<sup>50</sup> used a machine learning study to predict solute rejection performance by using solvent properties (dipole moment,  $\log P$  (partition coefficient), and the electronic state of the solvent) and solvent–solute structural information. For this purpose, the rejection of 407 solutes in 11 common and green solvents was determined *via* a medium-throughput cross-flow nanofiltration system using a polyimide (PI) membrane. The resulting model exhibited remarkable robustness across various solvents, notably methanol, and achieved an impressive root mean square error (RMSE) score of 0.123 and an  $R^2$  value of 71.4 when evaluated against 311 literature data points. This demonstrated the model's strong generalization capabilities beyond the OSN database.

Concerning ML studies, it is worth noting that the existing OSN literature contains limited data, and the results have been generated under varying conditions. Consequently, this data is often not suitable for utilization by ML approaches. Furthermore, publications in this field frequently concentrate solely on specific types of membranes, solvents, or solutes. Hence, there is an urgent need for an increased number of data to enhance data quality and consequently, improve model performance generated by ML approaches. Instead, ML studies are expected to advance the OSN field and open new avenues for research and development.

## 5.2. Quantitative evaluation of OSN performance

Upon a thorough examination of experimental OSN studies, it becomes evident that solvent viscosity ( $\eta_s$ ,  $\mu_s$ ) stands as the primary solvent property influencing solvent permeance ( $P_s$ ). In general, there exists an inverse relationship between  $P_s$  and  $\eta_s$  (Fig. 5a), which adheres to the Hagen–Poiseuille equation (eqn (1) or (2)).<sup>13</sup> However, it is essential to note that this equation is typically applied to membranes with uniform

cylindrical nanopores, where no substantial concentration gradient through the membrane is present. In the case of 2D nanolaminate membranes, eqn (2) is predominantly preferred.<sup>51</sup> Based on the Hagen–Poiseuille equations, the fluxes of different solvents can be qualitatively compared, initially considering the solvent viscosity. Another crucial factor to consider is the total Hansen solubility parameter ( $\delta$ ), which was initially used in polymeric membranes due to their potential for significant swelling during operation. However, since ceramic or GO membranes are resistant to swelling, it is deemed more appropriate to employ equations that exclude the parameter  $\delta$ .<sup>52</sup>

$$J = \frac{\varepsilon \pi r^2 \Delta P}{8 \eta \delta \tau} \quad (1)$$

$$J = \frac{h^4 \Delta P}{12 L^2 \eta \Delta x} \quad (2)$$

Here,  $J$  represents the membrane flux, and parameters of  $\varepsilon$ ,  $r$ ,  $\Delta P$ ,  $\eta$ ,  $\tau$ ,  $h$ ,  $L$ , and  $\Delta x$  denote the porosity of the membrane surface, average pore radius, transmembrane pressure, solvent viscosity, membrane tortuosity, interlayer spacing between adjacent laminates, average lateral dimension of the nanosheets, and thickness of the membrane, respectively.

Recent studies have revealed the existence of additional parameters significantly affecting solvent permeance. Notably, the solubility ( $\delta$ ), dielectric constant ( $\varepsilon$ ), and molecular diameter ( $d_s$ ) of the solvents emerge as crucial contributors to permeance. For instance, despite having comparable viscosities, acetonitrile typically exhibits higher permeance than acetone, owing to its smaller kinetic diameter.<sup>54</sup> It is noteworthy that all equations employed to calculate solvent permeance in recent studies include the combinations of these fundamental properties (Fig. 5b–e). The separation performance of 2D membranes is intricately linked to the ordered or disordered align-

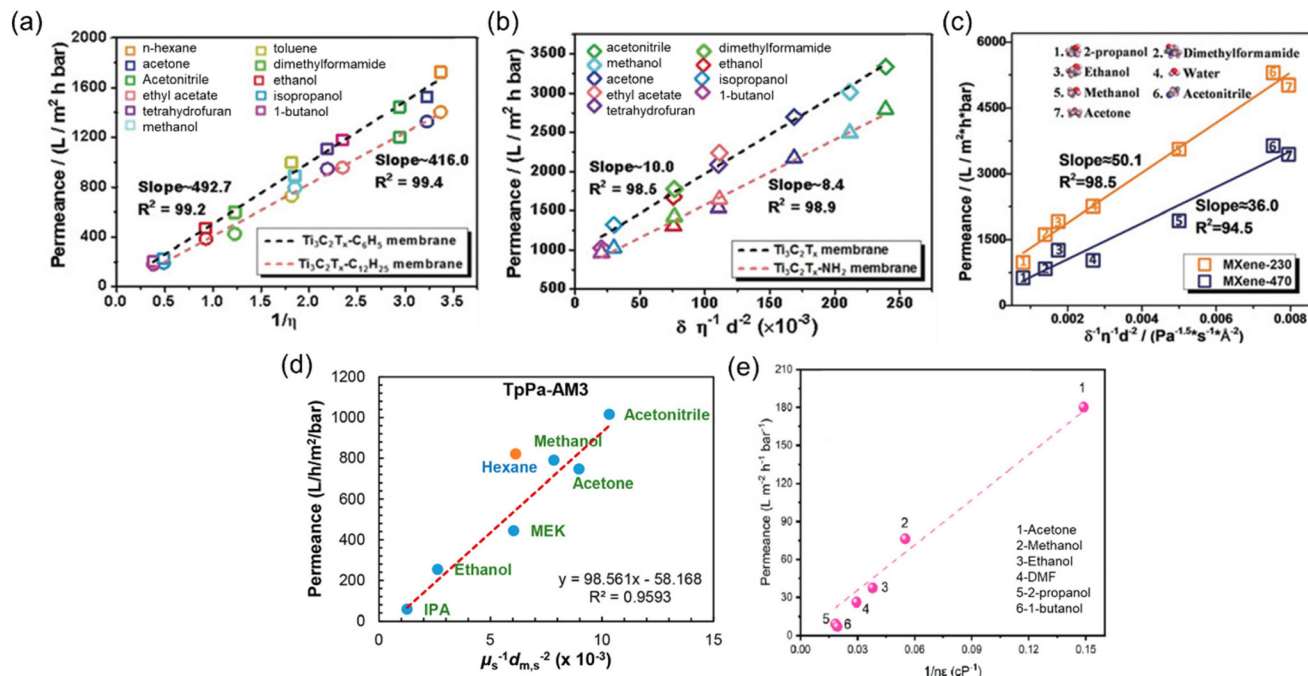


**Fig. 5** Solvent permeances against the combined solvent properties for (a) Ti<sub>3</sub>C<sub>2</sub>T<sub>x</sub>-C<sub>6</sub>H<sub>5</sub> and Ti<sub>3</sub>C<sub>2</sub>T<sub>x</sub>-C<sub>12</sub>H<sub>25</sub> membranes,<sup>53</sup> (b) Ti<sub>3</sub>C<sub>2</sub>T<sub>x</sub> and Ti<sub>3</sub>C<sub>2</sub>T<sub>x</sub>-NH<sub>2</sub> membranes,<sup>53</sup> reproduced from ref. 53 with permission from the Wiley Online Library, Copyright 2019. (c) MXene-230 and MXene-470 membranes,<sup>54</sup> reproduced from ref. 54 with permission from the Wiley Online Library, Copyright 2018. (d) Hydrophilic COF (TpPa-AM3) membrane,<sup>55</sup> reproduced from ref. 55 with permission from the American Chemical Society, Copyright 2019 and (e) COF-rGO membrane.<sup>56</sup> Reproduced from ref. 56 with permission from Elsevier, Copyright 2021.

ment of solvents within nanochannels.<sup>53</sup> This alignment primarily results from the interactions between the channels and the solvent molecules. Wu *et al.*<sup>53</sup> observed that polar solvents tend to orderly align within hydrophilic membranes, and their transport obeys the model equation of  $P_s = \delta_s/\eta_s \cdot d_s^2$  (Fig. 5b). In contrast, solvents with disordered configurations within the nanochannels of hydrophobic membranes follow a Hagen-Poiseuille equation of  $P_s = 1/\eta_s$  (Fig. 5a). On the other hand, an inverse-proportional relationship between  $P_s$  and  $\delta_s$  was observed for hydrophilic MXene membranes, so the equation was revised as  $P_s = 1/\delta_s \eta_s \cdot d_s^2$  (Fig. 5c).<sup>54</sup> However, for hydrophilic COF membranes, the equation of  $P_s = 1/\eta_s \cdot d_s^2$  was introduced, as the low solvent-membrane interaction in these membranes makes the solubility parameter insignificant for permeance (Fig. 5d).<sup>55</sup>

Rather than these highly combined parameters, in a study carried out by Sui *et al.*,<sup>56</sup> the Hagen-Poiseuille equation was extended to include the dielectric constant parameter. This extension was made since the dielectric constant of the solvent has a significant impact on the swelling and changes in the interlayer spacing of 2D membranes, which, in turn, greatly influences membrane performance. However, the contribution of the dielectric constant was found to be relatively weak, particularly with non-polar solvents like hexane, which exhibit weak interactions with the nanosheets. Nevertheless, the suitability of this parameter for polar solvents is demonstrated for the COF-rGO nanocomposite membrane in Fig. 5e.

Upon an examination of the equations designed for permeance assessment, it becomes evident that these equations exhibit variations depending on the specific characteristics of the solvent and membrane under consideration. In generalized research, it is reasonable to explore the development of an equation that contains the interaction energies between the membrane and solvent. To support this suggestion, the study of Liu *et al.*<sup>57</sup> can be given as an example. They conducted a series of measurements using two distinct COF membranes displaying high and low polarities. Remarkably, their investigations revealed that the high-polarity COF membrane exhibited high permeance in polar solvents, whereas the low-polarity COF membrane demonstrated lower permeance for the same polar solvents although it has a larger pore window. In contrast, this trend reversed when considering nonpolar solvents. In this case, the low-polarity COF membrane exhibited approximately five times higher permeance for non-polar solvents compared to its high-polarity counterpart. Similarly, Wu *et al.*<sup>53</sup> fabricated hydrophilic Ti<sub>3</sub>C<sub>2</sub>T<sub>x</sub> and hydrophobic Ti<sub>3</sub>C<sub>2</sub>T<sub>x</sub>-C<sub>12</sub>H<sub>25</sub> membranes. Notably, the hydrophilic MXene membrane exhibited a permeance to polar solvents at least 3.8 times greater than that of its hydrophobic counterpart, despite the latter having a larger interlayer spacing. This significant difference in permeance can be attributed to the robust interaction energy observed between the hydrophilic MXene membrane and polar solvents. This interaction induces an ordered configuration of polar solvents within the Ti<sub>3</sub>C<sub>2</sub>T<sub>x</sub> channels, resulting in enhanced permeance (see Fig. 6a and b). In the

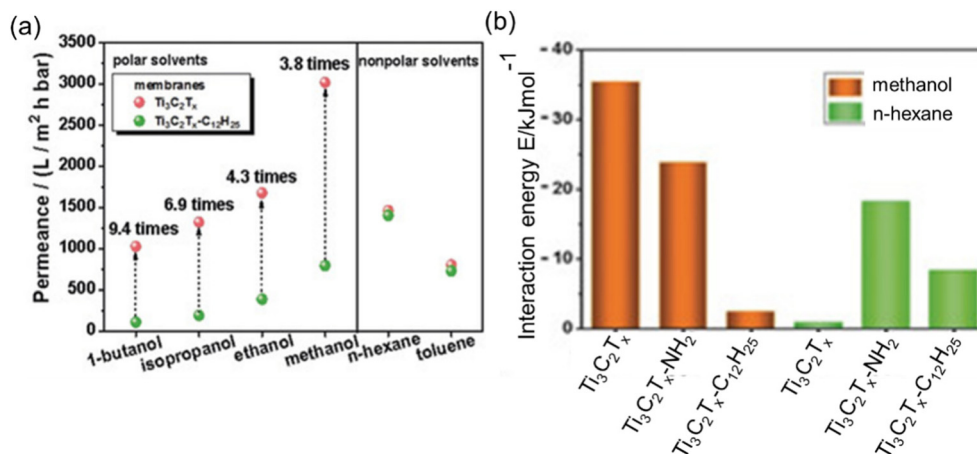


Fig. 6 (a) Comparison of hydrophilic Ti<sub>3</sub>C<sub>2</sub>T<sub>x</sub> and hydrophobic Ti<sub>3</sub>C<sub>2</sub>T<sub>x</sub>-C<sub>12</sub>H<sub>25</sub> membrane permeabilities, and (b) interaction energies between membrane and solvent.<sup>53</sup> This figure has been reproduced from ref. 53 with permission from the Wiley Online Library, Copyright 2019.

context of non-polar solvent permeation, it is noteworthy that there were notable similarities in permeances between the two distinct membranes under investigation. The observed consistency in performance can be ascribed to the analogous disordered structural arrangement of non-polar solvents within the nanochannels of both membranes, a phenomenon expounded upon through the utilization of molecular dynamics simulations. Collectively, the interaction energies between solvent and membrane defined from the molecular simulation studies would also be correlated with the performance of an OSN membrane. However, when it is desired to create an equation that includes solute molecules, it requires special attention since the equation becomes even more complex due to membrane-solute and solvent-solute interactions.

### 5.3. Standardized measurement conditions and evaluation of membrane stability

As highlighted earlier, the absence of standardized measurement conditions for the OSN process in laboratory tests hinders the safe comparison of OSN membranes as well as the elucidation of the exact separation mechanism. This concern is extensively discussed in a study conducted by Le Phuong *et al.*<sup>58</sup> Due to the variations in experimental conditions during OSN measurements, encompassing factors like temperature, pressure, solution and solvent concentration, and membrane thickness, among others, comparing results from different studies becomes a difficult task. For example, typical process parameters of OSN membranes range over 0.01–300 g L<sup>-1</sup> solute concentration, 0.1–800 h measurement time, 1–10 bar operation pressure, and 20–40 °C operating temperature. Additionally, as for solvent recovery measurements, alcohols represent the most favored solvent type, followed by polar aprotics and hydrocarbons. Regarding solute diversity, dyes are the most commonly used, followed by polystyrene, PEG, and pharmaceuticals, respectively. This complexity enhances the challenges within the already sophisticated OSN process. Therefore, it is crucial for researchers to follow the standar-

dized experimental conditions established by Le Phuong *et al.*<sup>58</sup> to safely compare the performance of OSN membranes while considering the collective insights of the research community.

The other standardized procedure may be the incorporation of long-term stability tests, which may serve as an important indicator of the suitability of OSN membranes for industrial separation applications. It is desired that an ideal membrane should consistently maintain peak performance over a long period without any performance loss. However, stability tests conducted in the literature thus far have been relatively short, often lasting no more than 7 days. Regrettably, these short-term assessments may not provide a comprehensive and realistic representation of a membrane's long-term stability.

The main reason for conducting short-term stability tests is that many well-established polymers are susceptible to swelling, dissolution, or degradation when exposed to organic solvents. Other challenges that polymeric OSN membranes face are physical aging caused by prolonged membrane lifespan, and membrane compaction under elevated operating pressure.<sup>59</sup> As a result, a dramatic loss in solvent separation performance of polymeric OSN membranes is observed. For instance, Kappert *et al.*<sup>60</sup> examined the swelling behavior of nine polymeric OSN membranes and reported how the swelling changes over a short-term period (0–8 hours) when exposed to 10 common solvents and evaluated the stability over a long-term period (up to 2 months) using spectroscopic ellipsometry. Accordingly, the overall conclusion was that there was no strict relation between swelling degree and solvent polarity or the structural similarity of polymers, and most of the polymers exhibited a swelling degree greater than 50%.<sup>60</sup> To offer a solution for the swelling of polymeric OSN membranes, common methods including crosslinking, surface modification, and the incorporation of nanofillers are identified.<sup>59</sup> In contrast, 2D or 3D nanomaterial-based membranes are generally recognized as more resistant to solvents compared to polymers. Short-term performance tests have shown that many 2D laminated membranes maintain their stability



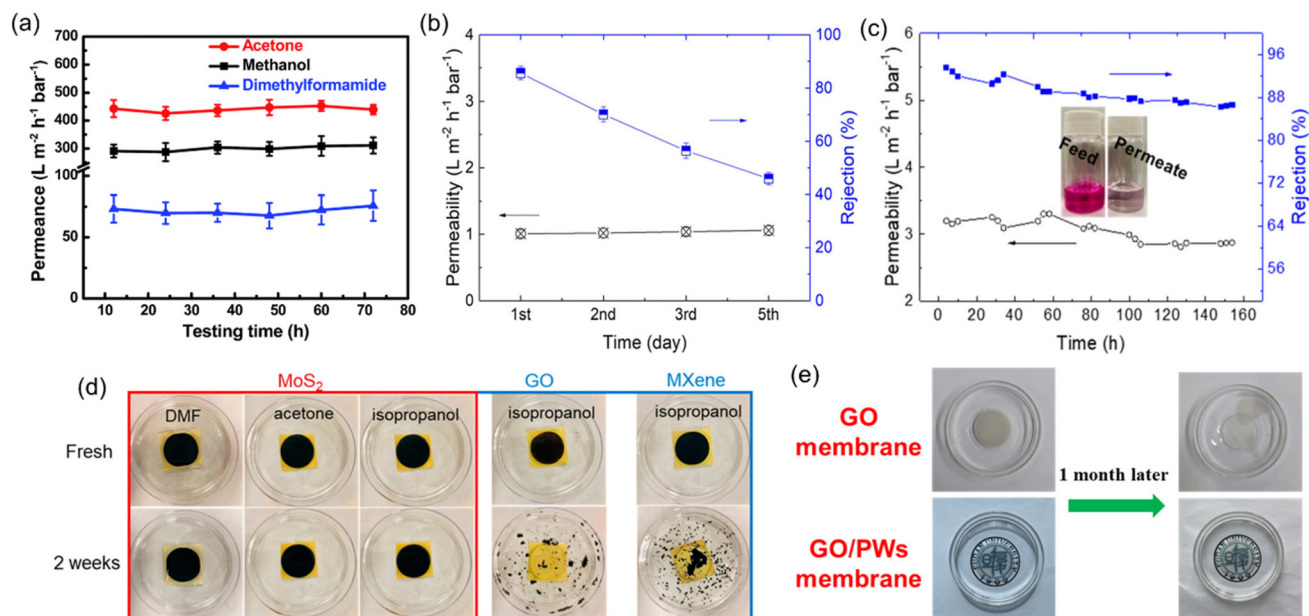


**Fig. 7** (a) Long-term solvent permeances of the GO-Si<sub>2</sub> membrane,<sup>61</sup> reproduced from ref. 61 with permission from the Royal Society of Chemistry, Copyright 2019. (b) Five-day isopropanol permeance and rejection to rose bengal of the chem-MoS<sub>2</sub> membrane,<sup>64</sup> (c) seven-day isopropanol permeance and rejection to rose bengal of the hydro-MoS<sub>2</sub> membrane,<sup>64</sup> (d) photographic evidence depicting the integrity of MoS<sub>2</sub>, GO, and MXene membranes in various solvents,<sup>64</sup> reproduced from ref. 64 with permission from the American Chemical Society, Copyright 2019 and (e) digital images illustrating the condition of GO and GO/polymeric nanowire (PW) membranes following immersion in methanol for one month.<sup>68</sup> Reproduced from ref. 68 with permission from Elsevier, Copyright 2022.

for up to 80 hours, with no significant loss in solvent permeance or solute rejection performance (see example in Fig. 7a).<sup>37,53,61–63</sup> However, in long-term performance tests, the presence of functional groups in 2D laminated membranes can render them susceptible to oxidation, leading to a decline in performance over time. For instance, Guo *et al.*<sup>64</sup> demonstrated that MoS<sub>2</sub> membranes produced through chemical exfoliation (chem-MoS<sub>2</sub>) exhibited instability and oxidation when exposed to ambient air for a long time. In long-term stability testing, a significant decline in the solute rejection performance of the chem-MoS<sub>2</sub> membrane was observed within just 5 days (Fig. 7b). To enhance membrane stability, MoS<sub>2</sub> membranes were synthesized using the hydrothermal method (hydro-MoS<sub>2</sub>), which offered advantages such as a reduced unstable metallic 1T phase content, larger lateral size, and shorter preparation duration. These hydro-MoS<sub>2</sub> membranes underwent a drying process with glycerol pretreatment to ensure selective solute rejection. Remarkably, the hydro-MoS<sub>2</sub> membranes sustained their performance with minimal compromise throughout the 7-day performance assessment (Fig. 7c). Contrary to oxidation phenomena, the presence of functional groups in 2D laminated membranes can increase the stability of a membrane by the strong interaction between functional groups or their crosslinking ability at high temperatures.<sup>65–67</sup>

In addition to the performance stability test, a structural stability test of the membrane should be included in the standardized measurement procedure. Hopefully, in lab-scale measurements, contrary to the performance stability test, it has been carried out lasting up to 30 days by immersing a mem-

brane in a solvent under static conditions. Changes in morphology are monitored using scanning electron microscopy (SEM), while the membrane's structural resistance to swelling is comprehensively examined by X-ray diffraction (XRD) analysis. These tests revealed that pure polymeric membranes were unable to maintain their structural integrity as they swelled,<sup>69</sup> while 2D nanomaterial-based membranes maintained their structural stability against many solvents even after 30 days.<sup>14</sup> However, it is noteworthy that two widely utilized 2D nanomaterials, GO and MXene, exhibited disintegration after only two weeks of exposure to isopropanol solvent. This can be attributed to the abundance of side groups in both GO and MXene, which readily interact with the hydroxyl groups present in isopropanol through intermolecular forces, rendering them relatively dispersible in the solvent. In contrast, the absence of such side groups in MoS<sub>2</sub> makes it a more suitable candidate for applications involving isopropanol solvent (Fig. 7d). Recent studies have aimed to address this structural stability issue in free-standing laminated membranes through methods like intercalation, the production of composite membranes, and the utilization of various cross-linking agents. These efforts have yielded promising results (Fig. 7e).

## 6. Performance metrics of 2D laminated membranes

The objective of this study is to elucidate the profound significance and functional role of free-standing 2D nanolaminate



membranes in the context of their performance for methanol separation. To realize this goal, we compiled the performance metrics of a diverse array of 2D nanomaterials, including carbon-based nanomaterials (such as graphene, GO, and rGO), COF, MXene, MoS<sub>2</sub>, boron nitride (BN), and a variety of other 2D nanomaterials (HfNb<sub>3</sub>O<sub>8</sub>, zeolite-templated carbons (o-2DZTC), vermiculite (VMT), nickel hydroxide (NH), tungsten disulfide (WS<sub>2</sub>), and diamond-like carbon nanosheets (DLC)). Furthermore, our study extends to encompass hybrid microstructures, which involve evaluations of 2D-0D, 2D-1D, 2D-2D, and 2D-3D nanocomposites. Our evaluation included an extensive set of over 45 solutes, characterized by a wide spectrum of molecular weights ranging from 98.1 to 1422 g mol<sup>-1</sup>, covering diverse categories of solutes such as dyes, antibiotics, and food additives. However, it is important to note that this comparative analysis does not contain such factors as membrane thickness, structural attributes, pore dimensions, interlayer spacings, the concentration gradient within hybrid 2D membranes, or the functionalization status of the membranes. The following figures given in this section present the compiled data for our review study, which draws upon various sources to determine the methanol recovery and solute enrichment performance of free-standing 2D nanolaminate membranes in OSN applications. Table S1 of the ESI† contains more detailed information and performance data for each specific study presented in these figures, facilitating readers to locate relevant papers or materials of interest. Given the inherent variability and complexities introduced by these numerous parameters, we avoided making direct quantitative comparisons among the diverse 2D membranes. Finally, we aimed to establish the performance boundaries—both upper and lower limits—that any 2D membrane can achieve regarding pure methanol permeance and solute rejection proficiency.

### 6.1. Pure methanol permeance

Permeance represents the quantity of solvent that can pass through the membrane. For simplicity, it is generally measured without any solute addition to the feed stream.<sup>1,32</sup> To emphasize the exceptional methanol separation performance of free-standing 2D OSN membranes, we have initially compiled data on their pure methanol permeance, drawing from different sources in the existing literature, as presented in Fig. 8a and b. The total number of studies examined for each type of 2D OSN membrane is given by the numbers at the top of the figure. Considering the compiled literature, it can be deduced that the scientific community has shown considerable interest in carbon-based (graphene/GO/rGO) and COF membranes, respectively, as prominent 2D membrane materials for methanol separation, with a total of 18 and 15 distinct studies, respectively. This substantial interest may be attributed to their earlier discovery relative to other 2D nanomaterials (COF in 2005<sup>55</sup> and GO in 1859<sup>70</sup>) and their economic viability, combined with the ability to modulate pore size and interlayer spacing. The following highly investigated nanomaterials for the OSN membrane are Ti<sub>3</sub>C<sub>2</sub>T<sub>x</sub> (member of the MXene family), MoS<sub>2</sub>, and BN. Recently, other 2D nanomaterials, including WS<sub>2</sub>, NH, HfNb<sub>3</sub>O<sub>8</sub>, VMT, o-2DZTC, and DLC, are undergoing extensive investigation to assess their potential in methanol separation. This trend underscores the ongoing expansion and progression of the 2D nanomaterial family for membrane application.

Comparing free-standing 2D nanolaminate OSN membranes given in Fig. 8a, carbon-based ones exhibited restricted and comparatively low pure methanol permeance across various studies, except for one exceptional case. These reduced methanol permeances in carbon-based membranes primarily

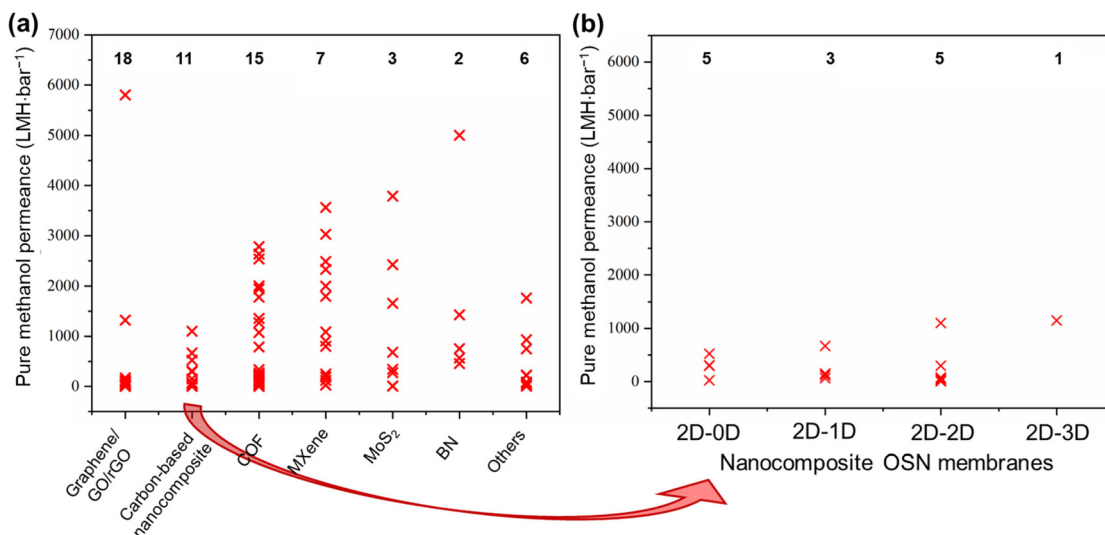


**Fig. 8** The pure methanol permeance of (a) 2D nanomaterials and carbon-based nanocomposites, and (b) mixed-dimensional nanocomposites based free-standing membranes (the numbers at the top of the figures represent the number of studies that examined 2D membranes, not the total data for each 2D membrane). Mixed-dimensional nanocomposite membranes in (b) are composed of carbon-based composite membranes and three other nanocomposite membranes.

result from the compaction of a one-atom-thick structure, occurring under high pressure. The application of pressure transforms the initially disordered nanosheets into a more ordered arrangement. Given the limited available space and the average interlayer spacing of approximately 1 nm between nanosheets, methanol permeance is significantly hindered.<sup>71</sup> An additional factor contributing to the low solvent permeance is the development of tortuous and extended pathways between the nanolayers in carbon-based membranes, which substantially increases flow resistance.<sup>72</sup>

Diverse strategies have been proposed to tackle these challenges, which include pore formation, flake size management, and composite membrane production. These methods have demonstrated promising outcomes by effectively reducing tortuosity and enhancing nanochannel size.<sup>14</sup> For instance, the development of nanoporous graphene membranes, commonly referred to as holey graphene (HG), has yielded promising results. Additional pores within the membrane were created by either ion irradiation, chemical etching, or nanoimprint lithography.<sup>14,73,74</sup> A noteworthy example is the work of Kang *et al.*,<sup>14</sup> who fabricated nanoporous graphene membranes through a sequential process involving thermal pore activation and microwave-assisted reduction of GO (Fig. 9a). These membranes exhibited the highest pure methanol permeance among all the examined 2D membranes, with an outstanding methanol permeance of 5800 LMH bar<sup>-1</sup>. Although it was directly attributed to the resulting reduced friction on the graphene surface due to the lower oxygen groups in the original paper, a closer look at the compiled data presented in Fig. 8a

reveals that the primary factor responsible for this effect is actually the formation of nanopores.

In addition to pristine carbon-based nanomaterials, carbon-based nanocomposites have also garnered substantial attention in OSN membranes, aimed at enhancing solvent permeance. To illustrate, Guo *et al.*<sup>75</sup> fabricated a GO-BN hybrid membrane to improve solvent permeance. This novel hybrid structure enables the creation of a more complex nanochannel structure characterized by diverse flake sizes and interlayer distances (Fig. 9b). The study yielded impressive results, with a methanol permeance of 1110 LMH bar<sup>-1</sup>, representing nearly a six-fold enhancement compared to pure GO OSN membranes.

Comparing free-standing 2D nanolaminate OSN membranes given in Fig. 8a, COF nanomaterials are ranked as the second most extensively studied 2D OSN membranes. They are crystalline, nanoporous 2D materials characterized by pore dimensions typically falling within the range of 0.5 to 4.7 nm.<sup>76</sup> These frameworks are constructed through the covalent bonding of organic linkers, a feature that allows for precise adjustment of pore sizes. This adjustment can be achieved by employing organic linkers of varying lengths or by introducing functional groups to these organic linkers. However, it is important to note that while such modification offers versatility, there is a limitation on the number of stable organic linkers available.<sup>77,78</sup> Instead, their comparable crystallinity and high porosity make them potential as a membrane material.<sup>79</sup>

COF OSN membranes exhibited a broad distribution of pure methanol permeances as illustrated in Fig. 8a, consistent with their large range of nanopore and nanochannel size

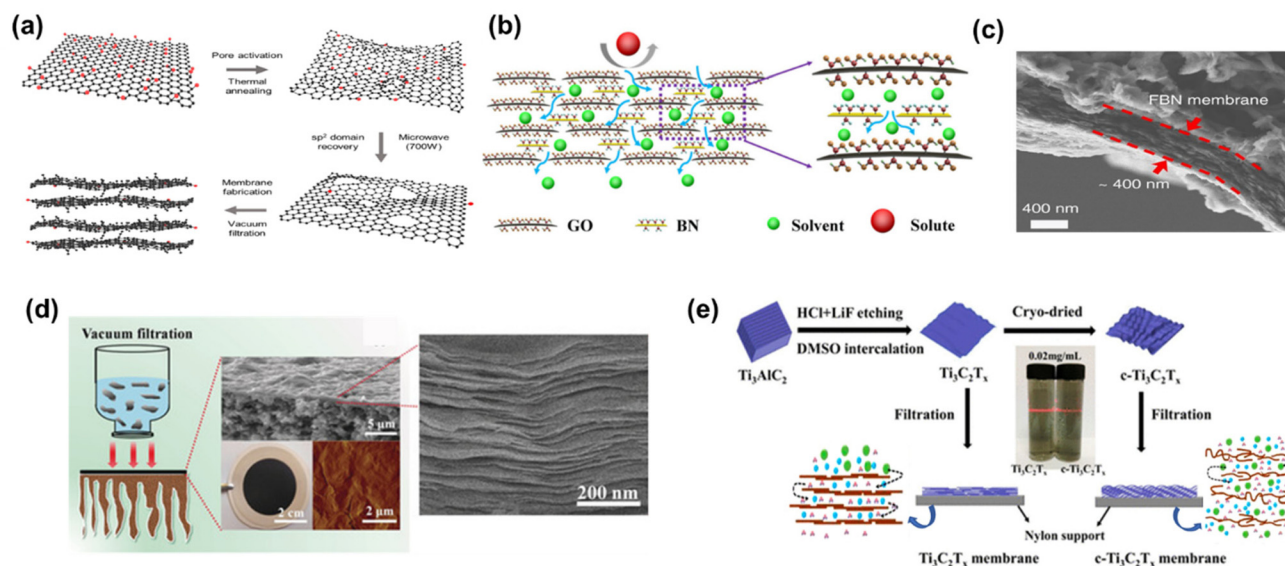


**Fig. 9** Schematic representation of (a) nanoporous multilayer graphene membrane,<sup>14</sup> (reproduced from ref. 14 with permission from the Springer Nature, Copyright 2023) and (b) GO-BN membrane,<sup>75</sup> (reproduced from ref. 75 with permission from the Springer Nature, Copyright 2023). (c) Cross-sectional SEM image of a FBN-0.4 membrane,<sup>16</sup> (reproduced from ref. 16 with permission from the Springer Nature, Copyright 2018). (d) MXene membrane preparation and the corresponding cross-sectional SEM image, and surface AFM image,<sup>54</sup> (reproduced from ref. 54 with permission from the Royal Society of Chemistry, Copyright 2018) and (e) preparation process and schematic representation of the Ti<sub>3</sub>C<sub>2</sub>T<sub>x</sub> and crumpled membranes (c-Ti<sub>3</sub>C<sub>2</sub>T<sub>x</sub>).<sup>15</sup> Reproduced from ref. 15 with permission from the American Chemical Society, Copyright 2020.

ensuring the solvent transport. Among them, a carboxylated COF (c-COF) membrane with a pore size of roughly 2.62 nm in a neutral environment was found to have the highest methanol permeance of 2785 LMH bar<sup>-1</sup>.<sup>80</sup> The objective of this particular study was to investigate the impact of solution pH, recognizing that solutions from industries such as food, chemical, petrochemical, and pharmaceutical may contain a variety of impurities, including acidic and basic components. The researchers observed a remarkable influence of pH variations on methanol permeance. Specifically, when subjected to low and high pH conditions, methanol permeance reduced to 2535 and 1780 LMH bar<sup>-1</sup>, respectively. Simulation outcomes indicated that the solvated pore size of c-COF was minimally affected by changes in the pH of a solution, while methanol diffusion was notably influenced by the solvated solute radii. In essence, they displayed that c-COF OSN membrane can maintain its performance in the altering pH of the feed solution, without changing its pore size.

Among all membranes compiled in Fig. 8a, amino-functionalized BN (FBN) membranes<sup>16</sup> seem to have the second-highest pure methanol permeance. This superior performance was primarily ascribed to their significantly reduced membrane thickness (Fig. 9c). However, it is crucial to note that the FBN membrane with a thickness of 400 nm had numerous defects and, as a result, was unsuitable for any solute separation application. Therefore, this exceptionally high methanol permeance could be misleading, given the presence of defects within the membrane structure. With the increase in thickness of the FBN membrane from 0.4 to 8 μm, additional nanolayers were added to mask the existing defects. This resulted in a substantial one-order-of-magnitude decrease in pure methanol permeance, reducing it from 5005 to 456 LMH bar<sup>-1</sup>. This clearly reveals the necessity of production of defect-free ultra-thin membranes, and ongoing research should be dedicated to this target.

Metal-containing structures like MXene<sup>53,54</sup> and MoS<sub>2</sub><sup>12,81</sup> membranes revealed large variations in pure methanol permeance. This can be attributed predominantly to the strength of interactions between the metal-containing surface of a membrane and solvent as well as adjustable interlayer spacing and structural morphology.<sup>12,16,53,54,81</sup> Maximum methanol permeance for MXene membranes was reported as 3563 LMH bar<sup>-1</sup>.<sup>54</sup> This remarkable performance is attributed to MXene's strong interaction with polar molecules like methanol, driven by its hydrophilic properties. Additionally, its rigid structure arising from the metal layer leads to regular and robust interlayer spacing (Fig. 9d). As a result, methanol tends to form regularly aligned clusters either on the surface or within the nanochannels of the MXene membrane, facilitating ultrafast solvent permeation. In contrast to MXene nanoplates, graphene or GO nanoplates are highly flexible, making it challenging to achieve uniform spacing between nanolayers. During the transport of methanol within GO nanochannels, collisions among methanol occur, leading to a reduction in permeance. In a recent study, the wrinkles and corrugations in GO were minimized by producing GO with larger flake sizes ranging

from 10 to 20 μm. The strong interlayer interactions between these larger overlapping areas resulted in the formation of slightly laminated nanochannels.<sup>82</sup> However, despite the GO membrane being much thinner (8 nm in thickness) compared to the MXene membrane (230 nm in thickness), its methanol permeance remains significantly lower than that of MXene (9.6 vs. 3563 LMH bar<sup>-1</sup>). The observed low methanol permeance of GO membranes, despite larger flake sizes, is indicative of non-uniform and reduced interlayer spacing between the nanolayers due to the lack of nanosheet rigidity. Additionally, it likely arises from the increased tortuosity for methanol transport towards the nanochannels of large GO nanoflakes, which emphasizes the necessity of the shift to the use of GO membranes with smaller flake sizes.<sup>83</sup> Collectively, metal-containing nanomaterials like MXene emerge as potential membrane materials over GO membranes.

Contrary to previous assertions put forth for GO, Xing *et al.*<sup>15</sup> demonstrated that crumpled MXene outperforms its flat counterpart with well-ordered structures (Fig. 9e). For comparison, they produced flat MXene membranes with a common vacuum filtration method and to induce crumpling in the MXene structure, MXene flakes underwent a freeze-drying process before the vacuum filtration. The resulting crumpled MXene exhibited remarkable permeance, reaching 2484 LMH bar<sup>-1</sup> with a mass loading of 0.1 mg cm<sup>-2</sup>. However, the numerous voids within the crumpled MXene led to a noticeable decrease in solute rejection performance. In response, the researchers increased the thickness of the crumpled MXene at the cost of reduced permeance, achieving a comparable permeance of 1089 LMH bar<sup>-1</sup> at a mass loading of 0.25 mg cm<sup>-2</sup> while maintaining acceptable solute rejection levels. Conversely, the highly ordered MXene structure demonstrated a methanol permeance of 121 LMH bar<sup>-1</sup> at a mass loading of 0.1 mg cm<sup>-2</sup>, which further declined to 32 LMH bar<sup>-1</sup> at a mass loading of 0.25 mg cm<sup>-2</sup>. This study serves as a compelling illustration of how the same structural modifications in different nanomaterials can yield a different alteration in methanol transport due to the inherent rigidity of nanolaminates.

The utilization of various types of 2D nanomaterials as OSN membranes is steadily increasing due to their exceptional performances. The competence of new types of 2D membranes such as WS<sub>2</sub>,<sup>84</sup> NH,<sup>85</sup> HNb<sub>3</sub>O<sub>8</sub>,<sup>86</sup> VMT,<sup>87</sup> o-2DZTC,<sup>88</sup> and DLC,<sup>89</sup> in this field has begun to be explored. Their performances are labeled as "others" in Fig. 8a. The DLC membrane exhibited the highest methanol permeance within this category, reaching 1764 LMH bar<sup>-1</sup>. This remarkable performance is attributed to its ultra-thin thickness of 10 nm, achieved through plasma chemical vapor deposition using acetylene precursors, resulting in reduced mass transfer resistance. When the membrane thickness was increased to 35 nm, methanol permeance decreased to 218 LMH bar<sup>-1</sup>.<sup>89</sup> Pure methanol permeance of the DLC membrane is followed by the o-2DZTC, WS<sub>2</sub>, NH, VMT, and HNb<sub>3</sub>O<sub>8</sub> 2D membranes, respectively. It is worth noting that the limited studies on the OSN separation performance of these membranes do not fully

reflect their true OSN potential. It is anticipated that as research progresses, their separation potentials will be clearly recognized.

Hybrid nanostructures, initially emerging to enhance the solvent permeance and its stability, particularly carbon-based nanocomposites, have evolved over time (see Fig. 8b). They have expanded to encompass a wide range of possibilities for membrane production, enabled by various nanostructure combinations. The aim here is to combine the superior properties of different nanostructures to achieve better performance. To illustrate, Zhang *et al.*<sup>63</sup> developed nanocomposite membranes, combining 2D rGO nanosheets and 1D nickel phosphate nanotubes (NPTs-rGO). Compared to a 1  $\mu\text{m}$ -thick rGO membrane with a permeance of approximately 1.35 LMH  $\text{bar}^{-1}$ , the NPTs-rGO composite membrane achieved a significantly higher methanol permeance of 670 LMH  $\text{bar}^{-1}$ . This marked improvement in permeance can be attributed to several factors. Firstly, the incorporation of 1D NPTs establishes additional pathways for solvent transport. Secondly, NPTs serve as intercalants, effectively increasing the interlayer spacing of rGO nanosheets, thereby reducing methanol transport resistance and improving permeance. Additionally, the robust covalent bonding between nanosheets and nanotubes increases the overall stability of the membrane and provides long-term performance.

Comparing the dimension alteration in the accompanying nanomaterial to 2D nanolaminates, a considerable change is figured out in Fig. 8b. Wu *et al.*<sup>84</sup> produced a  $\text{WS}_2$ -ZIF-8 (2D-3D nanocomposite) membrane, having the highest methanol permeance of 1150 LMH  $\text{bar}^{-1}$  among the investigated hybrid nanocomposite membranes. In this case, 3D ZIF-8 increased the interlayer spacing within the  $\text{WS}_2$  nanolaminate, providing a stable interlayer spacing through coordination bridges between ZIF-8 and  $\text{WS}_2$ . As a result, the ZIF-8- $\text{WS}_2$  membrane demonstrated exceptional resistance to methanol swelling behavior and stable nanochannel formation leading to high methanol permeance. Upon careful examination of Fig. 8b, it is evident that the performance ranking is as follows: 2D-3D nanocomposite > 2D-2D nanocomposite > 2D-1D nanocomposite > 2D-0D nanocomposite. The increase in the dimension of the accompanying nanomaterial results in the formation of more interconnected and open structures, which in turn creates a more effective permeation pathway for methanol transport. Therefore, given the bulkier structure of methanol relative to water molecules, its transport is enhanced due to the availability of a regular nanochannel opening in the membrane structure. Additionally, the increased surface area of the resulting membrane provides more active sites for methanol interactions, facilitating diffusion and consequently, increasing permeance. Therefore, similar to water molecules, the polar nature of methanol strengthens the interaction with negatively charged 2D OSN membranes, yielding a regular orientation of methanol molecules within nanochannels during transport.

Pure methanol permeance (PMP) is undoubtedly a crucial performance indicator for applications where methanol re-

cycling and/or solute retention from methanol are aspired. Most of the membranes presented in Fig. 8a and b utilize the advantages of 2D laminated membranes by reducing the membrane thickness, increasing porosity and/or enlarging the interlayer spacing in order to boost the solvent permeance. Nevertheless, permeance-enhancing modifications carry the risk of low solute rejection, and it is unfortunate that the solute rejection in methanol is not consistently reported for highly permeable membranes, thereby overlooking the impact of these modifications on methanol/solute selectivity. At this point, it is useful to discuss permeance-enhancing modifications that can be beneficial for increasing PMP over other solvents. Since it is an extensively studied solvent, water is selected for comparison. Fig. 10 illustrates the ratio of PMP to pure water permeance (PWP, if accessible) for free-standing 2D nanolaminate membranes given in Fig. 8a and b. The dashed line represents the inverse relationship between the viscosity of methanol and water, which can be considered as an upper bound. Although PMP is usually limited in carbon-based membranes (see Fig. 8), maximizing the formation of additional transport pathways seems to increase the selective transport of methanol. To illustrate, Nie *et al.*<sup>83</sup> obtained a considerably higher PMP/PWP when they utilized small-flake GO (with a mode area of 0.03  $\mu\text{m}^2$ ) compared with large-flake GO (with a mode area of 0.43–0.51  $\mu\text{m}^2$ ), benefiting from more straightforward transport pathways. On the contrary, Yang *et al.*<sup>82</sup> achieved a similar result by using large-flake GO (10–20  $\mu\text{m}$ ) but reducing the membrane thickness down to  $\sim 10$  nm. Unlike the thicker nanolaminates, solvent passage through nanometer-size pinholes within the flakes contributed to fast permeation in the case of ultrathin GO membranes.

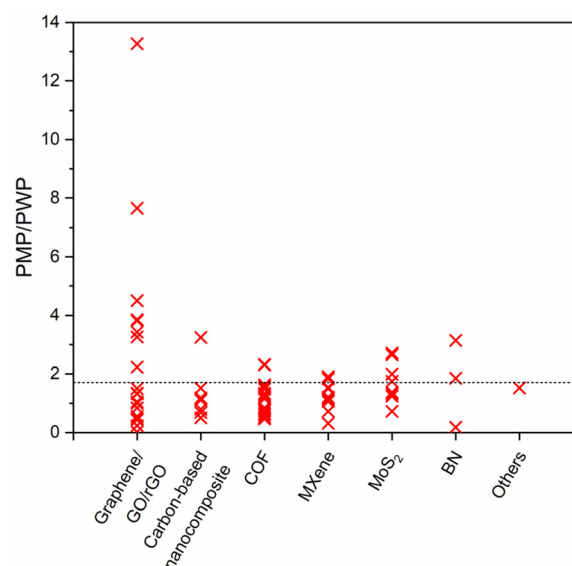


**Fig. 10** The ratio of pure methanol permeance (PMP) over pure water permeance (PWP) of free-standing 2D nanolaminate membranes. The dashed line represents the inverse relationship between the viscosity of methanol (0.54 mPa s) and water (0.916 mPa s). Raw data was given in Table S2.†



Another effective strategy to enhance PMP/PWP is the utilization of nanoporous graphene membranes. Kang *et al.*<sup>14</sup> showed that swelling behavior and separation performance of nanoporous graphene membranes fabricated by microwave-assisted reduction of graphene was “switchable” in response to solvent type, favoring the alcohol transport. Similarly, nanoporous multilayer GO membranes fabricated by Kim *et al.*<sup>90</sup> using slot-die coating and confined thermal treatment methods resulted in high PMP/PWP. Among carbon-based nanocomposites, intercalating multiwalled carbon nanotubes within lanthanum(III) ( $\text{La}^{3+}$ )-cross-linked small-flake GO nanosheets, thereby introducing low resistance transport pathways, was found to improve PMP/PWP in the work of Nie *et al.*<sup>91</sup> COF membranes were found to exceed the viscosity upper bound when a positive charge was introduced<sup>92</sup> or the pore size cut-off was adjusted to around 2.7 nm through slow annealing of the organic linkers.<sup>93</sup> On the other hand, the effect of tuning hydrophilicity or rigidity in MXene nanochannels on methanol transport is more evident compared with water transport. Wu *et al.*<sup>53</sup> demonstrated that highly hydrophilic neat and amine-functionalized  $\text{Ti}_3\text{C}_2\text{T}_x$  nanolaminates promoted the alignment of polar solvents as ordered molecular chains which facilitates fast methanol permeation. Harnessing the double-layered  $\text{Ti}_3\text{C}_2\text{T}_x$  nanosheets as rigid building blocks, uniform and rigid nanochannels of MXene membrane fabricated by Wang *et al.*<sup>54</sup> also surpassed the viscosity upper bound. Unlike the other 2D laminates in which ordered nanochannels enabled the solvent transport, loosely stacked  $\text{MoS}_2$  flakes in the work of Cui *et al.*<sup>12</sup> formed hierarchical, branching nanochannels where large cavities among the stacked flakes contributed to PMP while narrow gaps at the flake edges retained solute rejection. Lastly, utilizing charged BN nanosheets was found to have a positive effect on PMP/PWP compared with neat BN.<sup>94</sup> To generalize, it is possible to assert that discussed approaches such as introducing additional low-resistance transport pathways or expediting the inner-channel permeation through channel-solvent interactions may apply to all solvents. However, we illustrated that their effect is more apparent in terms of methanol permeance compared with water permeance. This can be attributed, in part, to the relatively low viscosity of methanol, which enables more effective utilization of the additional pathways. Furthermore, despite its high polarity, the limited number of hydrogen-bonding sites in methanol reduces the possibility of being retained by the nanochannel in case of favorable channel-solvent interactions. Ultimately, these strategies may be key to improve selective transport of methanol in free-standing 2D nanolaminate membranes.

## 6.2. Solute rejection on the basis of molecular weight

Rejection ( $R\%$ ), a critical parameter quantifying the retention of valuable solutes by OSN membranes, significantly impacts their performance.<sup>1,32</sup> To emphasize the efficacy of various free-standing 2D nanolaminate OSN membranes in terms of solute rejection, we initially demonstrated this data as a function of the molecular weight ( $M_w$ ) of solute in Fig. 11. Because

the corresponding study did not provide the relevant methanol permeance when the feed contains solutes. This figure offers a comprehensive insight into the solute rejection capabilities of diverse free-standing 2D nanolaminate membranes, including carbon-based membranes (graphene/GO/rGO), carbon-based nanocomposites, COF,  $\text{MoS}_2$ , BN, and other 2D membranes. It encompasses data from 45 distinct solutes, each characterized by a unique  $M_w$  spanning from 98.1 to 1422  $\text{g mol}^{-1}$ , representing a wide spectrum of industrial applications, from dyes to antibiotics and food additives.

In OSN, two key rejection mechanisms in solute rejection are at play: Donnan exclusion and size exclusion.<sup>95</sup> Yet, upon closer examination of 2D membrane rejection performance, it becomes clear that for  $R\% > 40\%$ , size exclusion predominantly governs solute rejection since the variation in solute rejection narrows with the increase in solute  $M_w$ . However, focusing on the region of  $R\% < 40\%$  in Fig. 11, it is obvious that complex triple interactions among the solute, solvent, and membrane significantly impact the overall separation process.

Wu *et al.*<sup>53</sup> conducted a comprehensive study to investigate how 2D OSN membranes reject dyes of varying sizes and charges. This research unveiled the intricate interplay of size, charge, and structural characteristics in shaping the separation efficiency of 2D membranes. The amine-functionalized MXene ( $\text{Ti}_3\text{C}_2\text{T}_x\text{-NH}_2$ ) membrane, positively charged and featuring an interlayer spacing of 1.28 nm, achieved impressive rejection rates exceeding 92% for dyes larger than 1.28 nm, irrespective of their charge (Fig. 12a). Hydrophobic  $\text{Ti}_3\text{C}_2\text{T}_x\text{-C}_{12}\text{H}_{25}$  membrane, with a negative surface charge and an interlayer spacing of 1.66 nm, achieved rejection rates exceeding 99% for dyes larger than 1.66 nm, similarly regardless of charge (Fig. 12a). On the other hand, as expected, in addition

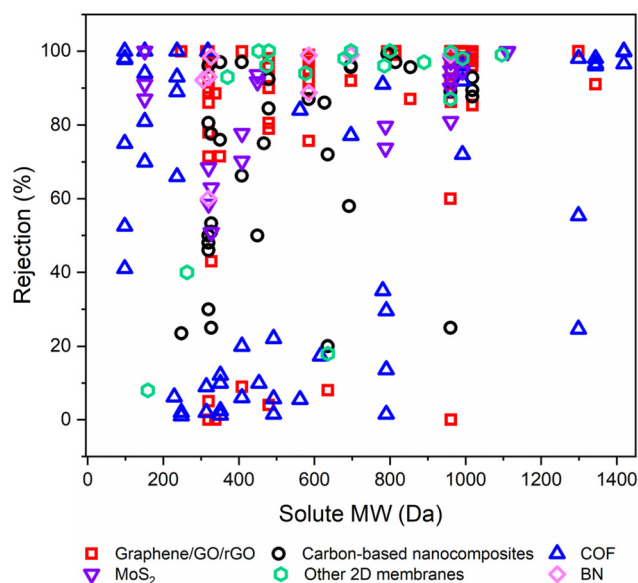


**Fig. 11** The solute rejection performances of various free-standing 2D nanolaminate OSN membranes as a function of the molecular weights of various solutes in methanol.

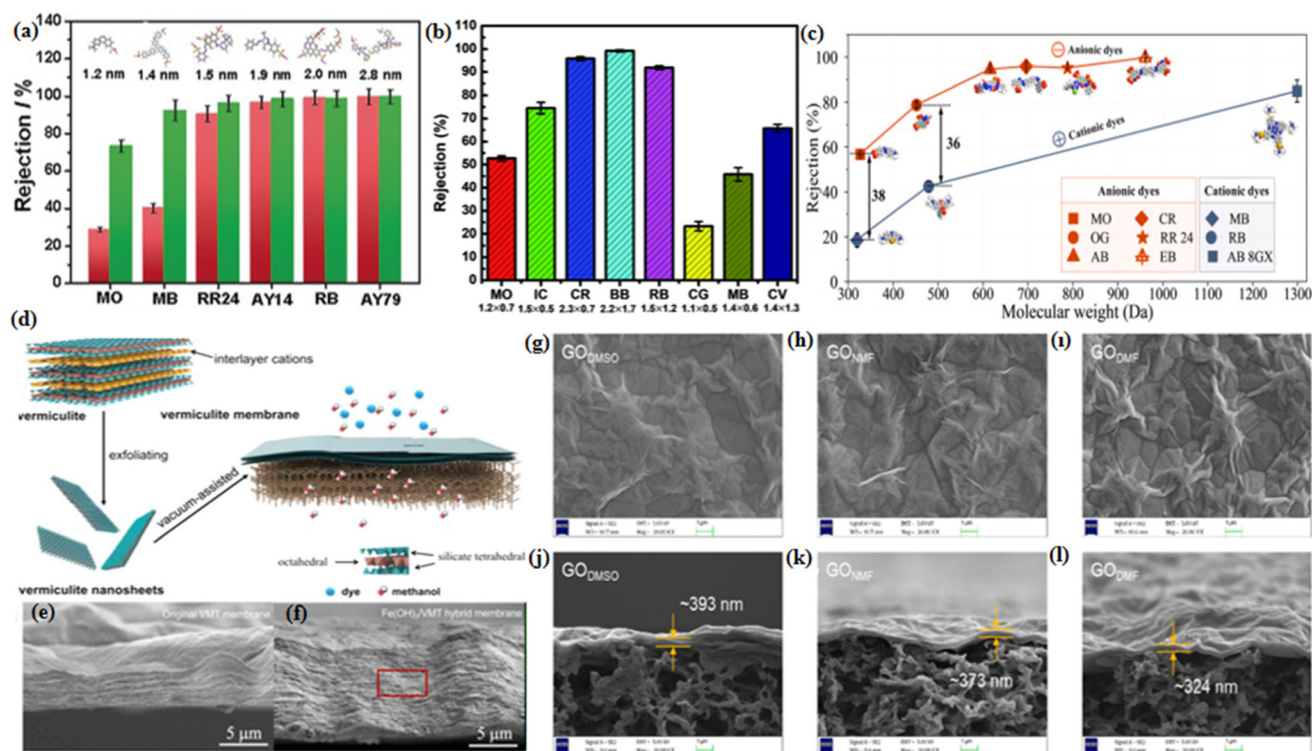


**Fig. 12** (a) Dye rejection of Ti<sub>3</sub>C<sub>2</sub>T<sub>x</sub>-NH<sub>2</sub> (green) and Ti<sub>3</sub>C<sub>2</sub>T<sub>x</sub>-C<sub>6</sub>H<sub>5</sub> (pink) membranes,<sup>53</sup> (reproduced from ref. 53 with permission from the Wiley Online Library, Copyright 2019). (b) GO-Si<sub>2</sub> membranes,<sup>61</sup> (reproduced from ref. 61 with permission from the Royal Society of Chemistry, Copyright 2019) where dyes are dissolved in methanol. The dyes used are methyl orange (MO), indigo carmine (IC), congo red (CR), brilliant blue R250 (BB), rose bengal (RB), chrysoidine G (CG), methylene blue (MB), and crystal violet (CV). The corresponding sizes (in nm) are mentioned either under or on their abbreviations. (c) Rejection performance of oi-COF membrane towards anionic and cationic dyes with varied molecular weights.<sup>11</sup> Anionic dyes: methyl orange (MO), orange G (OG), amido blue (AB), congo red (CR), reactive red 24 (RR24), evans blue (EB). Cationic dyes: methylene blue (MB), rhodamine B (RB), and alcian blue 8GX (AB 8GX). Reproduced from ref. 11 with permission from the Wiley Online Library, Copyright 2023. (d) Schematic illustration of the synthesis 2D lamellar VMT membrane.<sup>87</sup> Cross-sectional morphology of (e) pristine VMT, and (f) Fe(OH)<sub>3</sub>/VMT hybrid membrane.<sup>87</sup> Reproduced from ref. 87 with permission from the American Chemical Society, Copyright 2022. (g–i) Surface and (j–l) cross-sectional morphologies of GO<sub>DMSO</sub>, GO<sub>NMF</sub>, and GO<sub>DMF</sub> membranes, respectively.<sup>96</sup> Reproduced from ref. 96 with permission from the American Chemical Society, Copyright 2021.

to its size (1.4 nm) effect, for positively charged methylene blue (MB), the rejection was considerably low, 40% due to the attractive interactions between the membrane surface and the nature of MB. In contrast, the positively charged reactive red 24 (RR24) displayed an impressive rejection performance of 90%. In this case, the interplay between triple interactions starts to dominate. The findings of the simulation analysis of the current study indicate that the interaction between methanol and the membrane is relatively weak in comparison to the substantial interaction between methanol and the dye. Consequently, methanol induces a change in the configuration of the dye, leading to a more spread-out structure. This structural modification ultimately causes the membrane to exhibit improved rejection performance.<sup>53</sup> These findings emphasize that size exclusion primarily governs the rejection mechanism in 2D membranes, with Donnan exclusion playing a complementary role in dye separation.<sup>53,61,95</sup>

Depending on the membrane material type, the strength of solute–membrane interaction may play a dominating role in solute rejection, especially when the solute size is smaller

than the size of nanopore or nanochannel of a membrane. For instance, Wang *et al.*<sup>61</sup> suggested that a negatively charged GO-Si<sub>2</sub> membrane displayed significant solute rejection for negatively charged dyes and considerably lower performance with positively charged dyes (Fig. 12b). To investigate the effect of electrostatic interaction more comprehensively on dye rejection, rose bengal (RB) was compared to similarly sized, positively charged crystal violet (CV). RB achieved a rejection rate of 91.9% due to strong electrostatic repulsion, while CV had a 70% rejection rate, highlighting the role of electrostatic interactions. In a similar manner, Yuan *et al.*<sup>11</sup> synthesized negatively charged oriented ionic COF (oi-COF). The solute rejection analysis revealed a prominent role of size exclusion, with higher *M<sub>w</sub>* solutes being efficiently rejected. However, when comparing the rejection of negatively and positively charged dyes with smaller *M<sub>w</sub>*, the former exhibited significantly higher rejection rates (Fig. 12c). For example, orange G had a rejection rate of 78.7%, almost twice that of rhodamine B (42.4%), despite having a lower *M<sub>w</sub>* (452 vs. 479 Da). In summary, these

studies support the idea that for solutes with smaller  $M_w$ , electrostatic repulsion is the dominating factor for superior solute rejection.

Hopefully, the majority of 2D membranes in Fig. 11 exhibit remarkable performance in rejecting solutes with even small  $M_w$ . The rejection of solutes in 2D OSN membranes significantly improves as not only the size of dye molecules increases but also the size of nanochannel/nanopore decreases. This observation is particularly unsurprising for carbon-based 2D membranes, which display a very narrow interlayer spacing due to the compaction issues under pressure. This achievement of a narrow interlayer distance or small pore size can be observed in other 2D nanomaterials through membrane functionalization or intercalation procedures. For example, Shinde and colleagues<sup>97</sup> synthesized three distinct COFs, namely TFP-DPF, TFP-DNF, and TFP-DHF, with varying carbon chain lengths while sharing a similar structure. This led to COF membranes with different pore sizes: 1.22 nm for TFP-DNF, 1.41 nm for TFP-DHF, and 1.72 nm for TFP-DPF. Remarkably, the molecular weight cut-off (MWCO) of these COF membranes decreased from 1200 to 800 g mol<sup>-1</sup> as the pore size reduced from 1.72 to 1.22 nm. This highlights the potential for enhancing solute rejection, especially for small-molecular-weight solutes. This opportunity has resulted in the proposal of numerous COF structures in the literature. On the other hand, a range of intercalants, including carbon nanotubes, inorganic nanoparticles, and nanowires, are employed to tailor the distance of nanochannels in 2D membranes. However, the utilization of these intercalants is more appropriate when the  $M_w$  of the solute is high. To illustrate, Tian *et al.*,<sup>87</sup> conducted a study in which they intercalated Fe(OH)<sub>3</sub> nanoparticles within VMT nanosheets, comparing them to a pristine VMT membrane (Fig. 12d–f). The results were striking, with methanol permeance experiencing a remarkable 16-fold increase, rising from approximately ~30 to ~490 LMH bar<sup>-1</sup> without sacrificing the EB dye rejection performance, 99.7%.

Membrane preparation procedure also significantly plays a role in the final performance of a membrane. For instance, Zhang *et al.*<sup>96</sup> produced various GO membranes using different solvents: DMSO, NMF, and DMF, yielding GO<sub>DMSO</sub>, GO<sub>NMF</sub>, and GO<sub>DMF</sub> membranes with varying interlayer distances. Residual solvent trapped within the GO nanosheets acted as intercalant and led to a change in interaction energy and hence transition in the GO nanosheet conformation from a flat extended state to a wrinkled collapsed state (Fig. 12g–i). The rejection order for MB in methanol was GO<sub>DMF</sub> > GO<sub>NMF</sub> > GO<sub>DMSO</sub>, with rejection rates of 93, 89, and 86%, corresponding to *d*-spacing values of approximately 8.3 Å, 8.8 Å, and 9.1 Å, respectively. As anticipated, an increase in *d*-spacing corresponds to a reduction in dye rejection performance. This demonstrates that the membrane preparation procedure, specifically the choice of dispersive solvent acts as an intercalant and plays a critical role in solute rejection.

Considerations beyond adjusting the size of nanopore/nanochannel include accounting for changes in solute size

within the solvent, particularly taking into consideration the solvated solute radius. As previously discussed in section 5.1, Duong *et al.*,<sup>80</sup> investigated the effect of solution pH on the separation performance of c-COF membranes. They observed that the rejection of alcian blue (AB) from a methanol solution increased from 23 to 98% as the pH increased from 2.2 to 10.1. This advanced rejection performance was attributed by the outcome of simulations analysis to the variations in solute size at different pH levels. This conclusion can be also drawn from the knowledge that the solute solvated size undergoes a change when shifting between solvents, leading to varying rates of rejection for the same solute. This observation can be supported by the information observed from polymeric membranes, where a higher degree of chemical similarity between two solute molecules corresponds to closer rejection rates in a methanol solvent.<sup>50</sup>

### 6.3. Methanol permeance combined with solute rejection

Methanol separation is simultaneously governed by methanol permeance and solute rejection in the OSN process. Fig. 13 depicts the solute rejection *versus* methanol permeance of various free-standing 2D nanolaminate membranes collected from several studies. It is worth noting that a comprehensive comparison between 2D nanolaminate membranes remains elusive since in many studies the solvent permeance in the presence of a solute is not reported. Researchers engaged in OSN-related investigations are urged to emphasize the importance of addressing this issue. Concerning Fig. 13, the MoS<sub>2</sub> and COF membranes exhibit exceptional separation performance, characterized by both high methanol permeance and solute rejection. However, the methanol separation performance of the majority of 2D OSN membranes is populated above a rejection rate of 90% and in the range of 10–100 LMH bar<sup>-1</sup> methanol permeance. Unfortunately, it is worth emphasizing that this grouped data

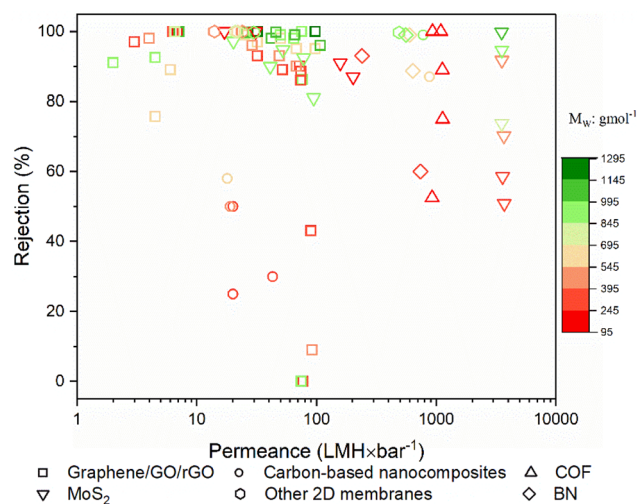


**Fig. 13** Solute rejection as a function of methanol permeance of various free-standing 2D nanolaminate OSN membranes. Colors indicate the molecular weight scale of solutes.



is produced using high  $M_w$  solutes (dominantly symbols with green color). With the decrease in  $M_w$  of solutes, rejection performance is hindered (see symbols with red colors on the lower part of the figure). Therefore, further improvements are necessary for free-standing 2D nanolaminate OSN membranes to effectively separate methanol, despite outperforming polymeric membranes.

If we are to offer an elaborate examination of each individual study that yields the most efficient membranes, one of the data in the right top corner of Fig. 12 belongs to the  $\text{MoS}_2$  membranes. This research, conducted by Cui *et al.*,<sup>12</sup> focused on the creation of hierarchical transferable nanochannels through the disordered stacking of irregular  $\text{MoS}_2$  flakes. These nanochannels featured narrow gaps (approximately 1.8 nm) at the contact edges of the flakes and large voids (about 8.3 nm) between the stacked flakes (Fig. 14a). Utilizing molecular dynamics simulations, they found that flow resistance in the large voids was lower than in the regularly structured voids, resulting in ultrafast methanol permeation at 3790  $\text{LMH bar}^{-1}$ . Simultaneously, the narrow gaps facilitated outstanding rejection rates of over 90% for solutes with kinetic diameters larger than 1.9 nm. However, as the solute size decreased, rejection performance decreased to approximately 50%. The hierarchical structure of the  $\text{MoS}_2$  membrane played a pivotal role in achieving this remarkable separation performance, offering high methanol permeance while maintaining comparable dye rejection.

COFs, shown in Fig. 13, rank second in separation performance, offering high solute rejection and relatively high methanol permeance. In a theoretical study performed by Wei *et al.*,<sup>55</sup> seven 2D COFs were systematically designed, varying functional groups, and adjusting aperture sizes (5.17 to 7.64 Å). Solute rejection in a methanol environment was evaluated using four solutes: 2,5-furan diamine (FDA), paracetamol (PRM),  $\alpha$ -methyl styrene dimer (MSD), and nile red (NRD). The outcomes revealed that solute rejection was intricately affected by several variables, encompassing solute size, solute polarity, aperture size, and membrane functionality (hydrophobic or hydrophilic). Generally, solute rejection decreased with larger COF apertures or smaller solutes, but solute polarity played a significant role. For example, despite a lower  $M_w$ , the highly polar PRM ( $M_w$ : 151.16  $\text{g mol}^{-1}$ ) outperformed the less polar MSD ( $M_w$ : 236.35  $\text{g mol}^{-1}$ ) (Fig. 14b). Moreover, it has been observed that while hydrophobic COF membranes had high solvent permeance, their solute rejection performance was comparatively low or equal in comparison to their hydrophilic counterparts (Fig. 14b and c). Additionally, the presence of solutes led to a reduction in solvent permeance compared to tests conducted with pure solvents. This is primarily attributed to pore clogging. For example, a hydrophilic COF's methanol permeance dropped from 1076 to 931  $\text{LMH bar}^{-1}$  in the presence of PRM solute, while that of hydrophobic COF decreased from 1356 to 1095  $\text{LMH bar}^{-1}$ . This study highlights the multifaceted factors influencing OSN membrane performance.

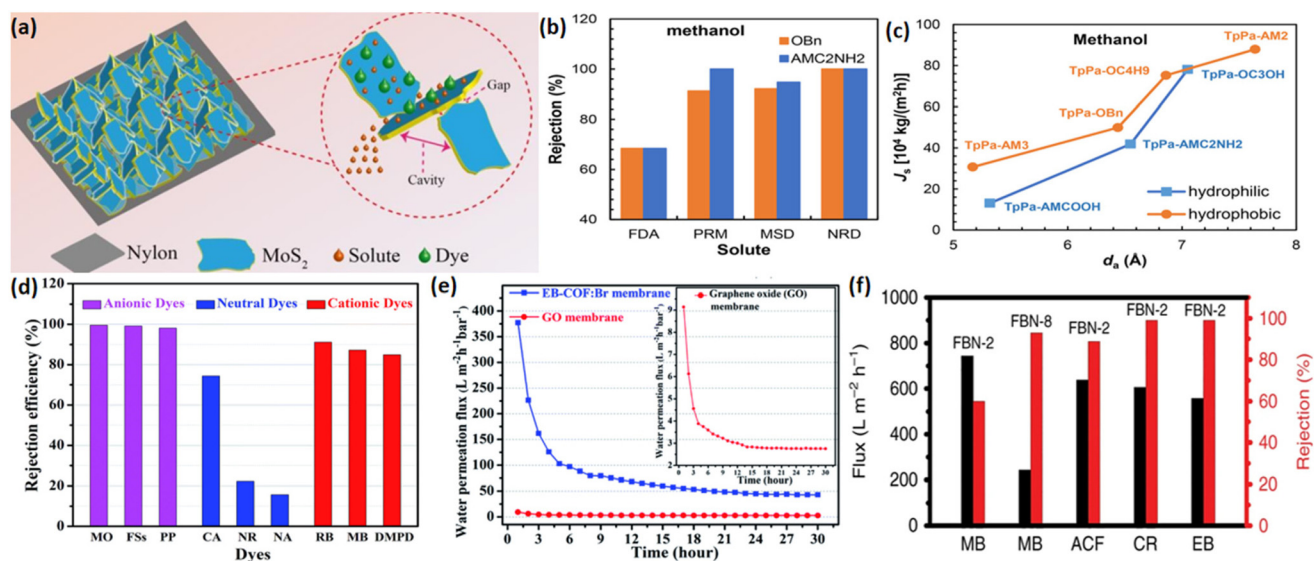


**Fig. 14** (a) Schematic representation of the hierarchical channels in the loosely stacked  $\text{MoS}_2$  membrane,<sup>12</sup> (reproduced from ref. 12 with permission from the Royal Society of Chemistry, Copyright 2019). (b) Solute rejection of hydrophobic TpPa-OBn and hydrophilic TpPa-AMC2NH2 membranes in methanol,<sup>55</sup> solutes: 2,5-furan diamine (FDA), paracetamol (PRM),  $\alpha$ -methyl styrene dimer (MSD) and nile red (NRD). (c) Solvent fluxes through the COF membranes as a function of aperture size,  $d_a$ ,<sup>55</sup> (reproduced from ref. 55 with permission from the American Chemical Society, Copyright 2019). (d) The rejection efficiency of the EB-COF:Br membrane for different dyes,<sup>92</sup> (anionic dyes: methyl orange (MO), fluorescein sodium salt (FSs) and potassium permanganate (PP); neutral dyes: nile red (NR), calcein (CA) and *p*-nitroaniline (NA), and cationic dyes: rhodamine B (RB), methylene blue (MB) and *N,N*-dimethyl-*p*-phenylenediamine dihydrochloride (DMPD)). (e) Water permeation flux of the EB-COF:Br membrane and GO membrane as a function of time,<sup>92</sup> (reproduced from ref. 92 with permission from the Royal Society of Chemistry, Copyright 2018) and (f) separation performance of FBN membrane *versus* molecular size of dyes in methanol solution<sup>16</sup> (methylene blue (MB), acid fuchsin (ACF), congo red (CR), evans blue (EB)) reproduced from ref. 16 with permission from the Springer Nature, Copyright 2018.



The other top-performing membrane was achieved through the surface modification of the COF membrane. Zhang *et al.*<sup>92</sup> synthesized a 2D cationic COF (EB-COF:Br) membrane through a Schiff base reaction, combining a cationic ethidium bromide (EB) monomer with 1,3,5-triformylphloroglucinol. Cationic dyes were effectively rejected by more than 85% due to electrostatic repulsion between the solute and membrane (Fig. 14d). Conversely, anionic dyes were immobilized within the membrane's pores, replacing them with Br ions through strong electrostatic attractive interactions between the positively charged pore walls of the membrane and anionic dye molecules. However, the immobilized solutes were not recoverable and led to reduced permeance by blocking the membrane pores. In cases where the electrostatic interaction between neutral dye molecules and the EB-COF:Br membrane was weak, rejection efficiency was controlled by the solute and membrane pore sizes. As the solute diameter increased (from 4.32 to 8.82 Å), solute rejection performance improved (from 15% to 74%) (Fig. 14d).<sup>92</sup> Similar observation is present for the other top-performing 2D OSN membrane, a 2 µm thick FBN membrane.<sup>16</sup> Solute separation follows the molecular size effect, with rejection rates of 60% for methylene blue (MB), 88.7% for amido black (ACF), over 99% for congo red (CR), and over 99% for evans blue (EB). Moreover, it maintained high solvent permeance in the presence of solute, ranging from 240–740 LMH bar<sup>-1</sup> (Fig. 14f).

Data presented in Fig. 13 does not represent the performance stability of free-standing 2D nanolaminate OSN membranes, which is crucial in the application of membranes to an industrial scale. It is well-known that the swelling effect of organic solvents presents a major challenge for 2D membranes, causing a gradual reduction in solute rejection performance and a fast increase in solvent permeance over time.<sup>98</sup> Unfortunately, the reported permeances do not accurately reflect the actual performance since they were observed before the membrane reached a stable state. Additionally, few studies reported the membrane performance stabilities by carrying out measurements ranging from a few hours to a maximum of 7 days. For instance, GO and silver nanoparticles-based nanocomposite (GO-Ag) membranes significantly enhanced membrane stability.<sup>99</sup> Additionally, this nanocomposite membrane maintained its structural integrity over an extended 70-day period, even when exposed to various environments, including aqueous, acidic, and basic conditions. Additionally, the composite membrane achieves exceptional dye rejection rates, exceeding 97%, while preserving a high methanol permeance of 530 LMH bar<sup>-1</sup>.<sup>99</sup> On the other hand, some membranes do not preserve their stabilities. For example, EB-COF:Br membrane lost its permeance dramatically and eventually reached equilibrium (Fig. 14e).<sup>92</sup> This decrease in permeance may be attributed to the slipping of COF layers, which, in the case of slipping, could lead to pore blockage and increased resistance against flow, resulting in reduced permeance.<sup>100</sup> Unfortunately, the permeances reported before the membrane reaches a stable state do not accurately reflect its actual performance. Therefore, research-

ers should pay close attention to reporting solvent permeance for 2D nanomaterial-based membranes that are able to compact (GO) or slip (COF).

## 7. Conclusion

Implementation of free-standing 2D nanolaminate nanomaterials to OSN membranes has led to a significant breakthrough in the field of separation techniques. This innovative approach offers a sustainable and cost-effective solution to the problem of industrial solvents contaminating the environment. Our mini-review study specifically focuses on the separation and recovery of methanol, a widely used solvent in industrial processes. Through the evaluation of various free-standing 2D nanolaminate OSN membranes, we have highlighted their potential to revolutionize separation processes in the industrial use of methanol. The various 2D OSN membranes are compared and discussed considering diverse parameters to emphasize their impact on different aspects.

Regarding the free-standing 2D nanolaminate OSN membranes, the performance of BN in terms of pure methanol permeance is impressive, exceeding 5000 LMH bar<sup>-1</sup>. However, we must be cautious, as the presence of defects or large pores could lead to a low solute rejection. On the other hand, COF, MXene, and MoS<sub>2</sub> membranes should be potentially evaluated as they offer a promising solution for fast methanol transport. These cutting-edge membranes are highly versatile, with the ability to be functionalized to alter the size of nanopore/nanochannel or to intercalate with specific molecules. Remarkable methanol permeances of a maximum of 3790 LMH bar<sup>-1</sup> were achieved. Contrarily, with a few exceptions, carbon-based membranes (graphene, GO, rGO) revealed restricted methanol permeance due to their ultrathin, flexible nanolayer. This can lead to compaction problems when subjected to high pressure. To overcome this issue, the researchers have proposed a promising strategy involving the production of hybrid nanostructures with carbon-based 2D nanomaterial and other nanomaterials having diverse dimensionality ranging from 0D to 3D. This results in a reduction in tortuosity and an increase in the size of nanopores/nanochannels, thus improving the methanol permeance from 120 LMH bar<sup>-1</sup> for the pristine carbon-based membrane to 1150 LMH bar<sup>-1</sup> for the hybrid membrane (WS<sub>2</sub>-ZIF8) when maximum values are concerned. It is imperative to note that the comparisons presented herein have not been made in accordance with any established measurement standard. In order to ensure accurate comparisons, it is essential to adhere to standardized test procedures (filtration time, solute concentration, pressure, temperature, *etc.*), particularly with respect to methanol measurements. As such, laboratory studies may be reliably integrated into industrial practices.

In order to evaluate the solute rejection performance of free-standing 2D nanolaminate OSN membranes, a diverse group of 45 solutes with molecular weights ranging from 98.1 to 1422 g mol<sup>-1</sup> was assessed. These solutes represent a broad

array of industrial applications, including dyes, antibiotics, and food additives. The data obtained from this assessment indicates that size exclusion is the dominant factor governing solute rejection, as the deviations in solute rejection diminish with an increase in molecular weight. Furthermore, the interplay of triple interactions among the membrane, methanol, and solute also plays a significant role in solute rejection, which is distinguished especially for the low molecular weight solutes. Based on the data of 2D OSN membranes, COF, MoS<sub>2</sub>, and carbon-based membranes appear to be highly viable candidates for separating solutes with low molecular weights. This observation is not surprising for carbon-based 2D membranes since they provide a very narrow interlayer spacing due to the compaction under pressure. Exhibiting both high methanol permeance and solute rejection, COF and MoS<sub>2</sub> membranes can be proposed as candidates for methanol separation. Apart from the ability of COF to vary in its pore size, the excellent performance of both COF and MoS<sub>2</sub> membranes is due to their electrostatic interaction with solutes. With a rejection of over 90% for a diverse group of solutes and a methanol permeance range of 10–100 LMH bar<sup>-1</sup>, the performance of 2D OSN membranes for methanol separation is impressive. It is expected that the ongoing studies on free-standing 2D nanolaminate membranes will lead to even better results in the future.

This study highlights the potential benefits of using advanced membrane materials such as 2D nanomaterials in improving the recovery of methanol and solute enrichment. However, to ensure the effectiveness of 2D nanolaminate OSN membranes, it would be advantageous for future research to consider conducting characterizations, performance tests, and computational studies that go beyond water and explore the solvents of interest. As we demonstrate using methanol as an example, the performance of free-standing 2D OSN membranes is closely related to the properties of the solvent. In many cases, interlayer spacing and swelling behavior of laminates vary from solvent to solvent, having a significant impact on the methanol permeance and solute rejection of the resulting membranes. This varying interlayer spacing, in combination with nanomaterial–solvent interactions, also modifies the orientation of methanol molecules within the confined space, further affecting the transport of methanol. Moreover, solvated solute radii, solvent-induced conformation of the solute molecule, and the Donnan exclusion mechanism, which is closely related to electrostatic interactions, lead to solute rejections varying from other solvents to methanol. Illustrated by our comparison of methanol with water, the effect of different modifications such as introducing additional transport pathways or expediting the inner-channel permeation through nanomaterial–solvent interactions can be more evident in terms of methanol permeance. To achieve optimal results with these innovative membranes, it is essential to maintain control over the size of nanopores, gain a comprehensive understanding of the selective mass transport mechanism that occurs within nanochannels, and realize a 2D membrane design specific to the solvent of interest.

On the other hand, although high performance has been achieved by free-standing 2D nanolaminate OSN membranes for methanol recovery, there is still a need to improve their long-term stabilities. Therefore, to enhance the reliability and durability of these membranes, it would be beneficial for future research to concentrate on investigating methods to improve their long-term structural and performance stabilities. Finally, another future direction should be to achieve practical applications of free-standing 2D OSN membranes. Therefore, it is crucial to focus on their large-scale production and ensure their successful transition from lab-scale to industrial-scale production.

## Conflicts of interest

There are no conflicts to declare.

## References

- 1 P. Marchetti, M. F. Jimenez Solomon, G. Székely and A. G. Livingston, *Chem. Rev.*, 2014, **114**, 10735–10806.
- 2 P. Biniaz, N. T. Ardekani, M. A. Makarem and M. R. Rahimpour, *ChemEngineering*, 2019, **3**, 8.
- 3 Toxics Release Inventory (TRI) National Analysis US EPA Online, <https://www.epa.gov/trinationalanalysis>, (accessed 14 January 2022).
- 4 G. Wypych, *Handbook of Solvents, Volume 2: Use, Health, and Environment*, ChemTec Publishing, Toronto, 2019.
- 5 F. G. Calvo-Flores, M. J. Monteagudo-Arrebola, J. A. Dobado and J. Isac-García, *Top. Curr. Chem.*, 2018, **376**, 1–40.
- 6 M. H. Davood Abadi Farahani, D. Ma and P. Nazemizadeh Ardakani, *Sep. Purif. Rev.*, 2018, **49**, 177–206.
- 7 M. Y. Zhou, Q. W. Su, W. H. Yu, L. F. Fang and B. K. Zhu, *J. Membr. Sci.*, 2023, **673**, 121409.
- 8 K. R. Balaji, R. Hardian, V. G. D. Kumar, R. Viswanatha, S. Kumar, A. Singh, M. S. Santosh and G. Szekely, *Mater. Today Chem.*, 2021, **22**, 100602.
- 9 S. Li, S. Liu, B. Su, X. Gao and C. Gao, *J. Membr. Sci.*, 2023, **685**, 121960.
- 10 A. Yao, D. Hua, Y. Hong, J. Pan, X. Cheng, K. B. Tan and G. Zhan, *ACS Appl. Nano Mater.*, 2022, **5**, 18718–18729.
- 11 J. Yuan, X. You, R. Zhang, Z. Yao, Q. Liu, L. Cao, S. Zhang, Y. Li, Z. Liu, Z. Jiang and H. Wu, *J. Membr. Sci.*, 2023, **688**, 122120.
- 12 X. Cui, X. Wu, J. Zhang, J. Wang, H. Zhang, F. Du, L. Qu, X. Cao and P. Zhang, *J. Mater. Chem. A*, 2019, **7**, 12698–12705.
- 13 L. Nie, C. Y. Chuah, T. H. Bae and J. M. Lee, *Adv. Funct. Mater.*, 2021, **31**, 2006949.
- 14 J. Kang, Y. Ko, J. P. Kim, J. Y. Kim, J. Kim, O. Kwon, K. C. Kim and D. W. Kim, *Nat. Commun.*, 2023, **14**, 1–13.
- 15 Y. Xing, G. Akonkwa, Z. Liu, H. Ye and K. Han, *ACS Appl. Nano Mater.*, 2020, **3**, 1526–1534.

- 16 C. Chen, J. Wang, D. Liu, C. Yang, Y. Liu, R. S. Ruoff and W. Lei, *Nat. Commun.*, 2018, **9**, 1–8.
- 17 L. Cseri, R. Hardian, S. Anan, H. Vovusha, U. Schwingenschlög, P. M. Budd, K. Sada, K. Kokado and G. Szekely, *J. Mater. Chem. A*, 2021, **9**, 23793–23801.
- 18 X. Yu, W. Fan, V. Wee, D. Shi, H. Yuan, Y. Ying, Y. Di Yuan, Z. Yang, Y. Feng, D. Sun and D. Zhao, *J. Membr. Sci.*, 2022, **644**, 120130.
- 19 P. Liu, J. Hou, Y. Zhang, L. Li, X. Lu and Z. Tang, *Inorg. Chem. Front.*, 2020, **7**, 2560–2581.
- 20 Y. Cheng, Y. Pu and D. Zhao, *Chem. – Asian J.*, 2020, **15**, 2241–2270.
- 21 J. Wang, J. Zhu, Y. Zhang, J. Liu and B. Van der Bruggen, *Nanoscale*, 2017, **9**, 2942–2957.
- 22 Methanol production capacity globally 2030, Statista, <https://www.statista.com/statistics/1065891/global-methanol-production-capacity>, (accessed 14 January 2022).
- 23 D. Roy, M. F. Wahab, M. Talebi and D. W. Armstrong, *Green Chem.*, 2020, **22**, 1249–1257.
- 24 D. Prat, A. Wells, J. Hayler, H. Sneddon, C. R. McElroy, S. Abou-Shehada and P. J. Dunn, *Green Chem.*, 2015, **18**, 288–296.
- 25 G. Szekely, M. F. Jimenez-Solomon, P. Marchetti, J. F. Kim and A. G. Livingston, *Green Chem.*, 2014, **16**, 4440–4473.
- 26 M. Galizia and K. P. Bye, *Front. Chem.*, 2018, **6**, 511.
- 27 J. F. Kim, G. Székely, I. B. Valtcheva and A. G. Livingston, *Green Chem.*, 2014, **16**, 133–145.
- 28 G. Székely, M. C. Amores de Sousa, M. Gil, F. Castelo Ferreira and W. Heggie, *Chem. Rev.*, 2015, **115**, 8182–8229.
- 29 I. Sereewatthanawut, F. W. Lim, Y. S. Bhole, D. Ormerod, A. Horvath, A. T. Boam and A. G. Livingston, *Org. Process Res. Dev.*, 2010, **14**, 600–611.
- 30 E. M. Rundquist, C. J. Pink and A. G. Livingston, *Green Chem.*, 2012, **14**, 2197–2205.
- 31 M. Mahbub, PhD thesis, Université de Lorraine, 2019.
- 32 R. W. Baker, Membrane Technology, in *Encyclopedia of Polymer Science and Technology*, California, 2002.
- 33 M. S. Suleman, K. K. Lau and Y. F. Yeong, *Chem. Eng. Technol.*, 2016, **39**, 1604–1616.
- 34 M. L. Liu, C. X. Zhang, M. J. Tang, S. P. Sun, W. Xing and Y. M. Lee, *Prog. Mater. Sci.*, 2023, **139**, 101162.
- 35 L. Ding, L. Li, Y. Liu, Y. Wu, Z. Lu, J. Deng, Y. Wei, J. Caro and H. Wang, *Nat. Sustainability*, 2020, **3**, 296–302.
- 36 M. Yi, F. Héraly, J. Chang, A. K. Kheirabad, J. Yuan, Y. Wang and M. Zhang, *Chem. Commun.*, 2021, **57**, 6245–6248.
- 37 L. Ding, Y. Wei, Y. Wang, H. Chen, J. Caro and H. Wang, *Angew. Chem., Int. Ed.*, 2017, **56**, 1825–1829.
- 38 Z. Wang, C. Ma, C. Xu, S. A. Sinquefeld, M. L. Shofner and S. Nair, *Nat. Sustainability*, 2021, **4**, 402–408.
- 39 K. R. G. Lim, M. Shekhirev, B. C. Wyatt, B. Anasori, Y. Gogotsi and Z. W. Seh, *Nat. Synth.*, 2022, **1**, 601–614.
- 40 Y. Lei, Y. Cui, Q. Huang, J. Dou, D. Gan, F. Deng, M. Liu, X. Li, X. Zhang and Y. Wei, *Ceram. Int.*, 2019, **45**, 17653–17661.
- 41 C. Chu, C. F. Fu, P. Zhang, T. Pan, X. Ai, Y. Wu, P. Cui, Q. Huang and J. Ran, *J. Membr. Sci.*, 2020, **615**, 118520.
- 42 Q. Long, S. Zhao, J. Chen, Z. Zhang, G. Qi and Z. Q. Liu, *J. Membr. Sci.*, 2021, **635**, 119464.
- 43 X. Yan, S. Cheng, C. Ma, J. Li, G. Wang and C. Yang, *J. Hazard. Mater.*, 2022, **422**, 126939.
- 44 M. Bastin, K. Hendrix and I. Vankelecom, *J. Membr. Sci.*, 2017, **536**, 176–185.
- 45 R. F. Fedors, *Polym. Eng. Sci.*, 1974, **14**, 147–154.
- 46 D. Bhanushali, S. Kloos and D. Bhattacharyya, *J. Membr. Sci.*, 2002, **208**, 343–359.
- 47 X. Li, Y. Liu, Q. Liu, Z. Zheng and H. Guo, *RSC Adv.*, 2022, **12**, 7189–7198.
- 48 M. Dahanayaka and J.-W. Chew, *ACS Sustainable Chem. Eng.*, 2022, **10**, 1499–1508.
- 49 J. Liu, Z. Zhao, L. Li, Y. Wu and H. He, *J. Membr. Sci.*, 2023, **677**, 121623.
- 50 G. Ignacz, N. Alqadhi and G. Szekely, *Adv. Membr.*, 2023, **3**, 100061.
- 51 W. Jin, G. Liu and N. Xu, *Organic-Inorganic Composite Membranes for Molecular Separation: Volume 5*, World Scientific Publishing Co., New Jersey, 2017.
- 52 A. Buekenhoudt, F. Bisignano, G. De Luca, P. Vandezande, M. Wouters and K. Verhulst, *J. Membr. Sci.*, 2013, **439**, 36–47.
- 53 X. Wu, X. Cui, W. Wu, J. Wang, Y. Li and Z. Jiang, *Angew. Chem., Int. Ed.*, 2019, **58**, 18524–18529.
- 54 J. Wang, P. Chen, B. Shi, W. Guo, M. Jaroniec and S.-Z. Qiao, *Angew. Chem., Int. Ed.*, 2018, **57**, 6814–6818.
- 55 W. Wei, J. Liu and J. Jiang, *ACS Sustainable Chem. Eng.*, 2019, **7**, 1734–1744.
- 56 X. Sui, Y. Wang, F. Liu, Z. Yuan, C. Wang, Y. Yu, K. Zhou, K. Goh and Y. Chen, *Matter*, 2021, **4**, 2953–2969.
- 57 J. Liu, G. Han, D. Zhao, K. Lu, J. Gao and T. S. Chung, *Sci. Adv.*, 2020, **6**(41), eabb1110.
- 58 H. A. Le Phuong, C. F. Blanford and G. Szekely, *Green Chem.*, 2020, **22**, 3397–3409.
- 59 Z. Wang, X. Luo, J. Zhang, F. Zhang, W. Fang and J. Jin, *Adv. Membr.*, 2023, **3**, 100063.
- 60 E. J. Kappert, M. J. T. Raaijmakers, K. Tempelman, F. P. Cuperus, W. Ogieglo and N. E. Benes, *J. Membr. Sci.*, 2019, **569**, 177–199.
- 61 S. Wang, D. Mahalingam, B. Sutisna and S. P. Nunes, *J. Mater. Chem. A*, 2019, **7**, 11673–11682.
- 62 T. Gao, L. Huang, C. Li, G. Xu and G. Shi, *Carbon*, 2017, **124**, 263–270.
- 63 L. Zhang, J. Wang, Y. Zhang, J. Zhu, J. Yang, J. Wang, Y. Zhang and Y. Wang, *J. Membr. Sci.*, 2022, **649**, 120401.
- 64 B. Y. Guo, S. D. Jiang, M. J. Tang, K. Li, S. Sun, P. Y. Chen and S. Zhang, *J. Phys. Chem. Lett.*, 2019, **10**, 4609–4617.
- 65 T. Hyun, J. Jeong, A. Chae, Y. K. Kim and D. Koh, *BMC Chem. Eng.*, 2019, **1**, 1–26.
- 66 M. Ding, H. Xu, W. Chen, G. Yang, Q. Kong, D. Ng, T. Lin and Z. Xie, *J. Membr. Sci.*, 2020, **600**, 117871.
- 67 A. Iakunkov and A. V. Talyzin, *Nanoscale*, 2020, **12**, 21060–21093.

- 68 Z. He, G. Liu, M. Huang, C. Wang, J. Hu and Y. Li, *Colloids Surf., A*, 2022, **654**, 130066.
- 69 Z. X. Low and J. Shen, *Sep. Purif. Technol.*, 2021, **256**, 117840.
- 70 G. S. Kamble, *Introductory Chapter: Graphene Oxide: Applications and Opportunities*, IntechOpen, London, 2018.
- 71 J. Y. Chong, B. Wang, C. Mattevi and K. Li, *J. Membr. Sci.*, 2018, **549**, 385–392.
- 72 H. M. Hegab, M. Ouda, P. Kallem, C. Aubry, Y. Ibrahim, F. Banat and S. W. Hasan, *Chem. Eng. J.*, 2022, **450**, 1385–8947.
- 73 W. Min, X. Chen, S. Huang, Y. Liao, Z. Liang, Y. Lei and J. Xu, *Carbon*, 2023, **210**, 118038.
- 74 C. Cheng, S. A. Iyengar and R. Karnik, *Nat. Nanotechnol.*, 2021, **16**, 989–995.
- 75 Q. Guo, M. Xu, Q. Tang, Y. Liu, W. Zhang, C. Guo, X. Zhao, Y. Zhu, S. Ye, D. Liu, W. Lei and C. Chen, *npj Clean Water*, 2023, **6**, 38.
- 76 X. Sun, M. Di, J. Liu, L. Gao, X. Yan and G. He, *Small*, 2023, **19**, 2303757.
- 77 X. Li, S. Cai, B. Sun, C. Yang, J. Zhang and Y. Liu, *Matter*, 2020, **3**, 1507–1540.
- 78 S. Kandambeth, K. Dey and R. Banerjee, *J. Am. Chem. Soc.*, 2019, **141**, 1807–1822.
- 79 Y. He, X. Lin, Y. Zhou, J. H. Chen, Z. Guo and H. Zhan, *Chem. Mater.*, 2021, **33**, 9413–9424.
- 80 P. H. H. Duong, Y. K. Shin, V. A. Kuehl, M. M. Afroz, J. O. Hoberg, B. Parkinson, A. C. T. van Duin and K. D. Li-Oakey, *Sep. Purif. Technol.*, 2022, **282**, 120028.
- 81 J. Ran, P. Zhang, C. Chu, P. Cui, X. Ai, T. Pan, Y. Wu and T. Xu, *J. Membr. Sci.*, 2020, **602**, 117963.
- 82 Q. Yang, Y. Su, C. Chi, C. T. Cherian, K. Huang, V. G. Kravets, F. C. Wang, J. C. Zhang, A. Pratt, A. N. Grigorenko, F. Guinea, A. K. Geim and R. R. Nair, *Nat. Mater.*, 2017, **16**, 1198–1202.
- 83 L. Nie, K. Goh, Y. Wang, J. Lee, Y. Huang, H. E. Karahan, K. Zhou, M. D. Guiver and T. H. Bae, *Sci. Adv.*, 2020, **6**(17), eaaz9184.
- 84 S. C. Wu, Y. Chen, X. Yan, X. J. Guo and W. Z. Lang, *Chem. Eng. J.*, 2022, **442**, 136139.
- 85 Y. Qu, Q. G. Zhang, F. Soyekwo, R. S. Gao, R. X. Lv, C. X. Lin, M. M. Chen, A. M. Zhu and Q. L. Liu, *Nanoscale*, 2016, **8**, 18428–18435.
- 86 K. Nakagawa, M. Kunitatsu, K. Yasui, T. Yoshioka, T. Shintani, E. Kamio, K. L. Tung, S. C. E. Tsang and H. Matsuyama, *J. Membr. Sci.*, 2021, **640**, 119799.
- 87 M. Tian, L. Wang, J. Wang, S. Zheng, F. Wang, N. Shao and L. Wang, *ACS Sustainable Chem. Eng.*, 2022, **10**, 1137–1148.
- 88 C. Kim, D. Y. Koh, Y. Lee, J. Choi, H. S. Cho and M. Choi, *Sci. Adv.*, 2023, **9**(6), eade7871.
- 89 S. Karan, S. Samitsu, X. Peng, K. Kurashima and I. Ichinose, *Science*, 2012, **335**, 444–447.
- 90 J. Kim, J. Kang, J. P. Kim, J. Y. Kim, J. H. Kim, O. Kwon and D. W. Kim, *Carbon*, 2023, **207**, 162–171.
- 91 L. Nie, K. Goh, Y. Wang, S. Velioglu, Y. Huang, S. Dou, Y. Wan, K. Zhou, T.-H. Bae and J.-M. Lee, *ACS Mater. Lett.*, 2023, **5**, 357–369.
- 92 W. Zhang, L. Zhang, H. Zhao, B. Li and H. Ma, *J. Mater. Chem. A*, 2018, **6**, 13331–13339.
- 93 K. Dey, S. H. Kunjattu, A. M. Chahande and R. Banerjee, *Angew. Chem., Int. Ed.*, 2020, **59**, 1161–1165.
- 94 M. Xu, Q. Tang, Y. Liu, J. Shi, W. Zhang, C. Guo, Q. Liu, W. Lei and C. Chen, *ACS Appl. Mater. Interfaces*, 2023, **15**, 12524–12533.
- 95 Y. Zhang, D. Chen, N. Li, Q. Xu, H. Li, J. He and J. Lu, *ACS Appl. Mater. Interfaces*, 2022, **14**, 10237–10245.
- 96 M. Zhang, P. Li, M. Li, W. Zheng, G. Xie, X. Xu, C. Liu and J. Jia, *J. Membr. Sci.*, 2021, **640**, 119841.
- 97 D. B. Shinde, L. Cao, A. D. Dinga, X. Li, S. Kumar, X. Liu, M. N. Hedhili, A.-H. Emwas, M. Addicoat, K.-W. Huang and Z. Lai, *Chem. Sci.*, 2020, **11**, 5434–5434.
- 98 Z. Yin, Z. Lu, Y. Xu, Y. Zhang, L. He, P. Li, L. Xiong, L. Ding, Y. Wei and H. Wang, *Membranes*, 2021, **11**, 621.
- 99 S. Sharif, K. S. Ahmad, F. H. Memon, F. Rehman, F. Soomro and K. H. Thebo, *Mater. Res. Innovations*, 2021, **26**, 373–381.
- 100 S. T. Emmerling, R. Schuldt, S. Bette, L. Yao, R. E. Dinnebier, J. Kästner and B. V. Lotsch, *J. Am. Chem. Soc.*, 2021, **143**, 41.